EXPERIMENTAL AND NUMERICAL INVESTIGATION OF SUPERCRITICAL FLOW INSTABILITY IN TWO VERTICAL HEATED PARALLEL CHANNELS USING CO_2.

By

Anantvir Singh Saini

A Thesis submitted to the Faculty of Graduate Studies of
The University of Manitoba
In Partial Fulfillment of the Requirements of the Degree of

MASTER OF SCIENCE

Department of Mechanical Engineering
University of Manitoba
Winnipeg, Manitoba

Abstract

Supercritical flow instability in two vertical heated parallel channels was investigated experimentally and numerically using the Supercritical flow facility-Vertical (SFF-V) and a licenced 1-D non linear code CATHENA v3.5.4.4.

The experiments were conducted with a range of system pressures from 7.4 to 9.1 MPa, inlet temperatures from 7 to 31 °C and various outlet k-factors. The working fluid used was CO_2 driven via natural convection instead of a pump due to economic reasons. Total 16 cases of supercritical flow instability were obtained.

The CATHENA code v3.5.4.4 was used to numerically model the instability boundary of the current experiments and also previous experiments conducted in China. The effect of wall thermal heat storage on instability boundary was also studied.

Acknowledgement

I would like to express my sincere thanks to my advisor, Dr. V. Chatoorgoon for the invaluable guidance and opportunity to work on this project. I would also like to thank my committee members Dr. P. Ferguson and Dr. R. Derksen, for their helpful comments and suggestions. I am grateful to Sviatoslaw Karnaoukh for technical support. I am also grateful to AECL for their financial support in this project. Finally, I would like to thank my family and friends for their support, guidance and patience.

Table of Contents

List of Tables

List of figures

Nomenclature

$\boldsymbol{m}$**in**(**exp**)	measured mass flow rate [kg s-1]	ΔP	measured pressure-drop
$\boldsymbol{\rho}$	density [kg m-3]	ΔPf	frictional pressure-drop
P	system pressure [MPa]	ΔPl	local pressure-drop
Tpc	pseudo-critical temperature [°C]	ΔPg	gravitational pressure-drop
$\boldsymbol{N}$**spc**	sub-pseudo-critical number	G	mass flux [kg m-2s-1]
$\boldsymbol{N}$**tpc**	true trans-pseudo-critical number	H	height of section [m]
β	isobaric thermal expansion coefficient [K-1]	L	length of section [m]
Cppc	constant pressure specific heat [J K-1 kg-1]	D	hydraulic diameter of section [m2]
hpc	pseudo-critical specific enthalpy [KJ kg-1]	g	gravity [m s-2]
hin	specific enthalpy at the inlet (experimental) [KJ kg-1]	fr	friction factor
Qin(exp)	electrical power (experimental) [kW]	Subscript	
Q heat	heating power [kW]	pc	Pseudo-critical
		in	inlet

Chapter 1 Introduction

1.1 Nuclear Energy

The demand for electrical energy will inevitably increase with the world's growing population. According to a report by the United Nations (World Population Prospects:2017) world population will grow from 7.6 billion in 2017 to 9.8 billion by 2050. In 2017, the global energy demand increased by 2.1% compared with 0.9% in 2016. Most of this demand was driven by developing countries, such as India and China. More than 70% of this energy demand was met by fossil fuels, a quarter by renewables and the remainder by nuclear energy (IAE, 2018). Thus, the world saw a rise of 1.4% in CO_2 emissions in the year 2017, an increase of 460 million tonnes (Mt), reaching a historic high of 32.5 gigatons.

One can say that in the future, the dependence on fossil fuels will increase to meet the energy demand of the growing population. However, there are major issues with using fossil fuels as a primary source of energy; the first and foremost is the increase of greenhouse gasses (GHG) emissions; secondly, fossil fuels are non-renewable sources of energy and their continued use will deplete the world's natural reserves, thereby hindering future generations from using these resources.

GHG can have serious consequences on the environment, such as global warming and ozone layer depletion. Hence, the minimization of the consumption of fossil fuels is desirable. Renewable resources such as solar, water and wind energy are great alternatives for clean energy generation. However, their reliability and efficiency depend on the geography.

Additionally, solar power plants are in the developmental phase and are currently expensive to set up, considering the cost of solar panels and the vast amount of land needed. Because the sun does

not shine all day, cost-effective ways must be found to store the electricity for night use when most electricity is needed. Likewise, wind energy also has its share of problems such as noise pollution and the requirement of large acres of land.

Nuclear energy is another alternative source for generating electricity and has been used since the 1950s. Those initial reactors were called 'Generation I' reactors. With progress in nuclear engineering, the reactors became more reliable and safer. Nuclear power plants produce less air pollution than fossil fuels and are more efficient than solar, water and wind energy alternatives. However, the nuclear waste produced by nuclear reactors is still a major problem. According to the report, Nuclear Power in the World Today (World Nuclear association, 2019), about 11% of the world's electricity is provided by 450 nuclear reactors in 30 countries. However, most of the reactors are Generation II and Generation III. In 2001, scientists from ten countries formed the Generation IV International Forum (GIF) and proposed six new advanced reactor designs that focused on sustainability, increasing efficiency, waste reduction and economic competitiveness .The six new proposed designs are Gas-cooled Fast Reactor (GFR), Lead-cooled Fast Reactor (LFR), Molten Salt Reactor (MSR), Supercritical Water-cooled Reactor (SCWR), Sodium-cooled Fast Reactor (SFR), and Very High Temperature Reactor (VHTR). Out of the six new designs, the Supercritical Water-cooled Reactor (SCWR) is being researched in Canada.

1.2 Supercritical Water-cooled Reactor (SCWR)

SCWR uses light water at supercritical pressure conditions ($P \geq 22.06$ MPa and $T \geq 373.946$ °C) as the working fluid. This high pressure and temperature increase the efficiency of the SCWR to about 44% or more, compared to 36% from Generation 2-3 reactors. The SCWR utilises a direct thermodynamic cycle as the fluid exiting the core is discharged directly to the high-pressure turbine through pipes. Thus, the use of a reactor pump may be avoided. Figure 1.1 shows the

schematic of a SCWR concept. Under normal operating condition, only two pumps are required: the feed water pump and the condensate extraction pump. As a result, the SCWR concept becomes more compact, simplified and economical.

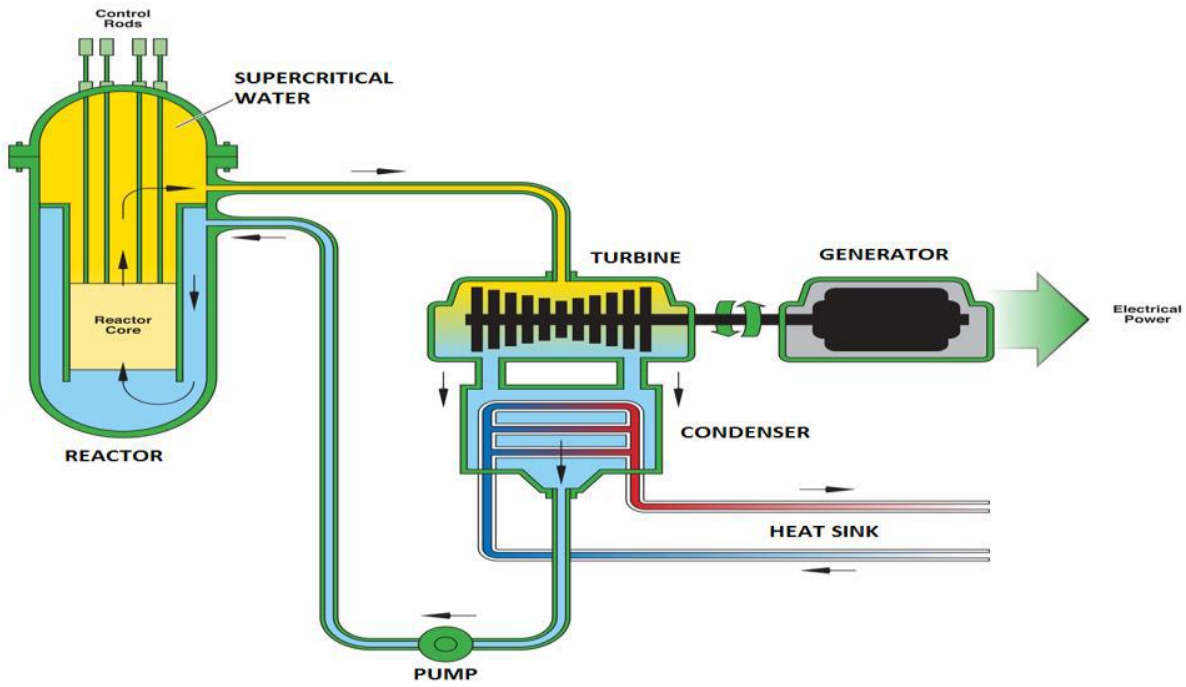

Figure 1.1: Schematic of SCWR design (OECD 2000)

The Canadian SCWR is a pressure-tube light-water concept that evolved from the CANada Deuterium Uranium (CANDU) heavy-water reactor (Leung and Nava-Dominguez, 2017). The core of the Canadian SCWR consists of an inlet plenum, 366 fuel channels installed through the tube sheet located at the bottom of the reactor vessel and an outlet plenum that merges with the inlet plenum. Figure 1.2 shows the core design of the Canadian SCWR concept. The light water from the feed water-pump is injected into the inlet plenum through four water lines and enters the fuel channels. After entering the fuel channels, the coolant flows down and reverses its direction

at the bottom of the fuel channels before turning upwards towards the outlet plenum. The coolant is then discharged to the high-pressure turbine via pipes.

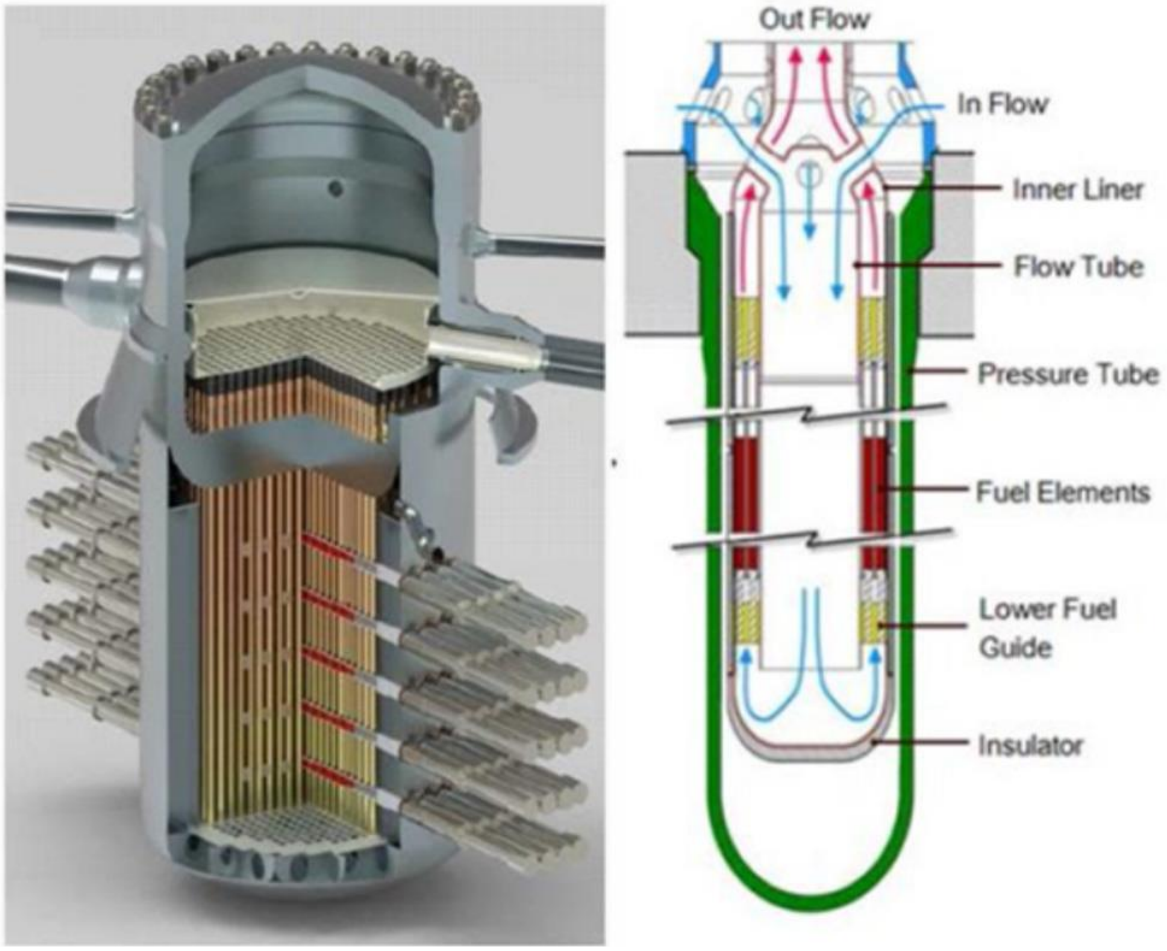

Figure 1.2: Schematic of the core of Canadian SCWR concept (Leung and Nava-Dominguez,2017)

The conceptual SCWR design offers potential benefits in terms of efficiency, better economics and will have high indexes of fuel usage in terms of thermal output per mass of fuel; thus, it will produce less nuclear waste. However, several technological challenges are associated with the development of the SCWR, such as the heat transfer, material chemistry, hydrodynamic instability

and demonstration of the passive safety systems. Because of these challenges, research into the development of the SCWR is ongoing. According to the Technology Roadmap Update for Generation 4 Nuclear Energy Systems (GIF), January (2014), the demonstration phase of the SCWR is estimated to start around 2025, followed by another ten years to finalize the details, and then the SCWR are expected to be available for commercial construction.

1.3 Supercritical fluids (SCF(s))

Any fluid can be characterized by a critical point, which is obtained at specific conditions of pressure and temperature. When a fluid is subjected to a pressure and temperature higher than its critical point, the fluid is said to be "supercritical". Figure 1.3 represents the phase diagram of H_2O.

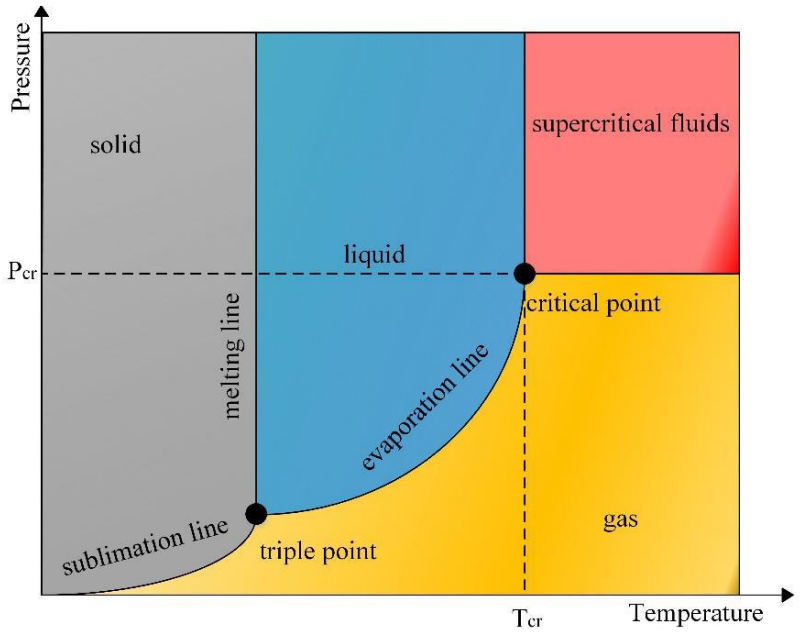

Figure 1.3: Phase diagram of H_2O

Above the critical point there exits a region called the supercritical region. In this region, the supercritical fluid exits as single phase having unique properties of both gas and a liquid. At any given pressure in this region, there is a corresponding temperature at which the fluid specific heat-

capacity, C_p, has a maximum value. Other properties such as density (ρ), viscosity (μ) and thermal conductivity (λ) also experience a drastic change when the working conditions approach this point, which is called pseudocritical point. The pseudocritical line, shown in the figure 1.4 is a plot of all the pseudocritical points in the supercritical region.

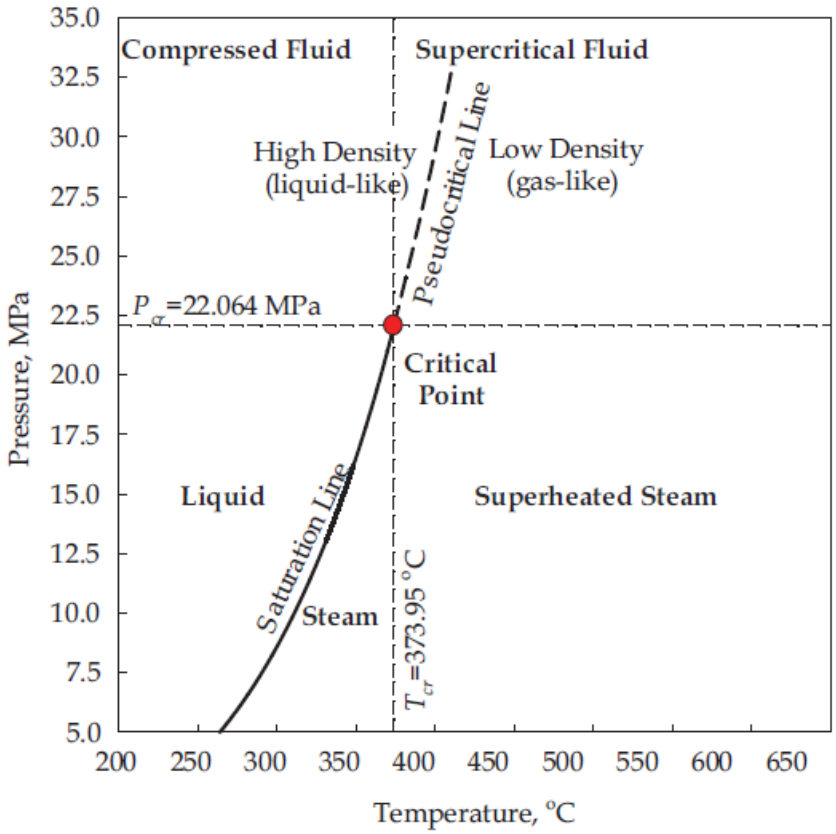

Figure 1.4: Phase diagram of H_2O showing pseudocritical line.

1.4 Supercritical Water

The critical point of H_2O corresponds to a pressure of 22.064 MPa and a temperature of 373.95 °C and exists as liquid and vapor at equilibrium. When water is heated above this temperature and pressure, water changes into a single-phase liquid without any boiling and the phase interface completely disappears. The properties of the supercritical fluid changes drastically on reaching the pseudocritical point, as shown in figure 1.5

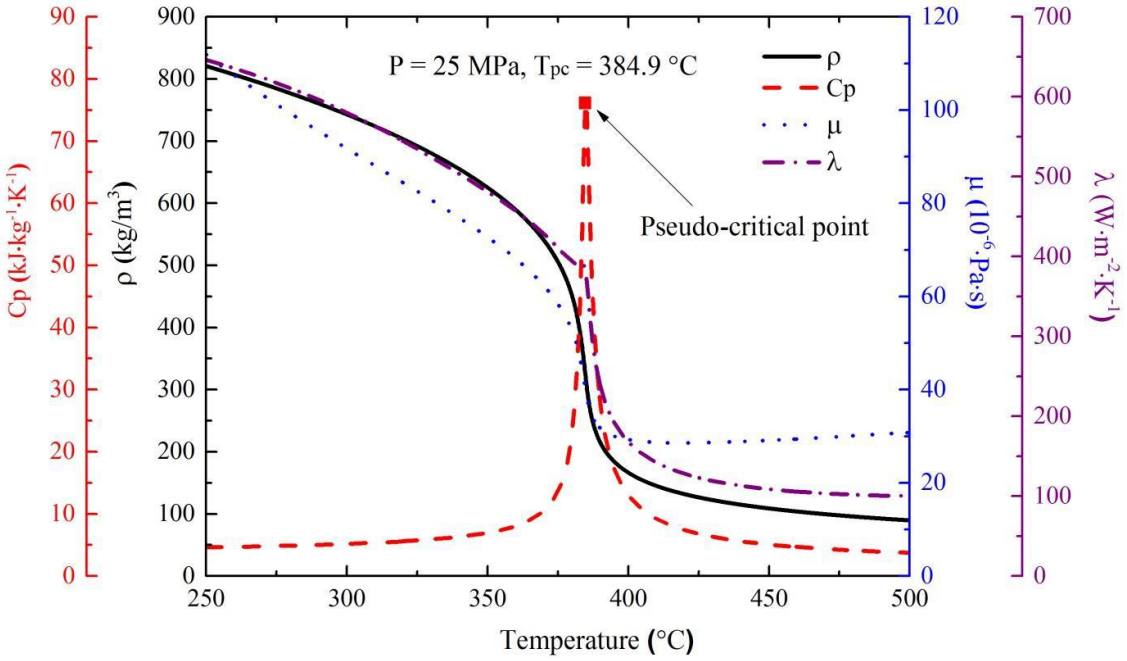

Figure 1.5: Supercritical H_2O properties at 25 [MPa].

1.5 Supercritical flow instabilities.

Despite the benefits of using SCF(s) as a coolant in the SCWR, the large changes in thermo-physical properties of SCF(s) may lead to thermal-hydraulic instabilities. Previous studies (Chatoorgoon, 2007; Xiong et al., 2012; Xi et al., 2014a) have show that instability can occur due to the feedback effect between the flow rate and pressure drop, which is caused by the effects of large compressibility in the supercritical thermodynamic region. These instabilities in a nuclear reactor must be avoided as sustained oscillation may lead to mechanical vibrations, degrade system control and can damage the reactor vessel. It is, therefore, necessary to understand the physical mechanism of these flow instabilities and to obtain instability boundaries before designing a prototype of Supercritical Water-cooled Reactor.

1.6 Research Objectives

The present study focuses on obtaining instability boundary data for Parallel Channel Instability (PCI) in heated parallel channels with vertical up-flow. The experimental facility used is a two vertical heated channel loop in which CO_2 is circulated with the use of natural convection forces. The objectives of the study are as follows:

1) Capture parallel channel instability data under different working conditions such as system pressure, inlet temperature and various outlet k-factors.
2) Obtain the power and mass flow rate at which PCI occurs.
3) Assess the ability of the CATHENA code v.3.5.4.4 to model the instabilities.
4) Study the effect of wall thermal energy storage effect on the instability using the CATHENA code, v.3.5.4.4.

Chapter 2 Literature Review

2.1 Flow Instability.

Flow instabilities in any industrial system may occur during operation and can drastically affect the flow behaviour, performance and efficiency of the system and are, hence, undesirable. The concept of flow instability dates to the nineteenth century. Many methods were developed to analyse this phenomenon, such as Reynolds number, Euler's equation, and Naiver-Stokes equations. With the modernization of technology, the analysis methods also evolved. The use of computers to model and analyse flow instabilities started in the 1980s. In general, flow instability may occur owing to disturbances in the upstream, depending on the nature of the flow parameters and system parameters. If the disturbance grows in amplitude with time, the flow is deemed unstable. If the disturbances damp or die with time, the flow is said to be stable. The flow instability phenomenon in supercritical flow has received a lot of attention in the last decade. The reason being the newly proposed Supercritical Water-Cooled Reactor (SCWR) design, which uses water at supercritical conditions as a coolant.

SCWR is one of the six new reactor designs proposed by the Generation IV International forum in 2001(DOENE (USDOE Office of Nuclear Energy, Science and Technology (NE)), 2002). During normal operation, water enters the core at 350 °C and leaves the core at 625 °C at a pressure of 25 MPa (Chow, 2008).

The core design of the SCWR consists of many parallel channels connected to common headers at the inlet and the outlet (Leung and Nava-Dominguez, 2017). Hence, it is necessary to study the flow behaviour in heated channels to get more insight into the flow dynamics.

2.2 Flow instabilities in heated channels with supercritical conditions.

Many researchers have numerically studied supercritical flow instabilities in heated channels. The literature mainly consists of three kinds of approaches. Out of the three, two are theoretical analyses with frequency domain method (FDM) and time domain method (TDM), and the third is experimental. 1-D and 3-D codes have been used for theoretical analyse of supercritical flow instability and are abundant in the open literature. On the other hand, there are limited number of reported experimental studies due to the expense of conducting experiments.

This literature review focuses on the stability of heated channels under supercritical pressure conditions.

Analytical study of supercritical flow instability was first started by Zuber (1966). He focused on the thermally induced oscillations experienced in rocket engine heat exchangers, which utilised oxygen and hydrogen at both subcritical and supercritical pressures. Two-region model with "liquid like region" and "gas like region" was proposed and analyzed. Three mechanisms; variation of the heat transfer coefficient, large compressibility and variation of fluid density near the pseudo-critical region were distinguished, which led to unstable operation. Finally, stability maps were constructed for defining the areas of stable operation.

Yi et al. (2004) developed a mathematical model to study the thermal-hydraulic stability of supercritical-pressure light water reactor. The code was developed using linearized one-dimensional, single-channel, single phase model. The study concluded that increasing the orifice pressure drop coefficient at the inlet, by decreasing the power to flow ratio, or decreasing the inlet temperature could stabilize the system

Zhao et al. (2005) proposed a three-region model for stability analysis at supercritical pressure. The regions consisted of “heavy fluid region”, “heavy and light fluid region”, and “light fluid region”. The mechanism of single channel density wave based on the three-region model was discussed and a characteristic equation was derived. Based on this characteristic equation, stability maps were generated using the pseudo sub-cooling number and expansion number. Parametric effects such as the effect of inlet orifice, inlet mass flow, system pressure, and inlet temperature on the single channel stability were assessed.

Ambrosini (2007) modeled a uniform heated channel with RELAP5/MOD3.3 code and analysed flow instability under boiling and supercritical conditions. The results showed that there exists an analogy between the density wave oscillations in both subcritical and supercritical flow. Ambrosini and Sharabi (2007) proposed new non-dimensional parameters and analyzed the stability of a heated channel with supercritical fluids. The new non-dimensional parameters, trans-pseudo-critical number and sub-pseudo-critical number used the pseudo-critical point as the only reference state. Moreover, these parameters do not consider the effect of heating structures and focuses mainly on thermal hydraulic behaviour. Using three different analysis tools, which included a system code, an in-house linear code and transient analysis program, Ambrosini and Sharabi (2010) assessed the flow stability boundaries in single heated channel with different supercritical fluids (H_2O, CO_2, R23, NH_3). The new non-dimensional parameters provided nearly the same stability threshold for the addressed system with different supercritical fluids.

Sharabi et al. (2007) used the FLUENT CFD code and modeled a single heated channel having cross section area and heating power comparable with those of the proposed SCWR subchannels. This analysis was done to check if the instability phenomenon predicted by an in-house linear analysis program, and RELAP5/MOD3.3 were also predicted well by the CFD code. Standard k-

ϵ model with wall functions and the low-Reynolds number model were used in this analysis. They concluded that both the standard k-ϵ model and the low-Reynolds number model were able to predict the onset of unstable behaviour with close agreements to the 1-D models.

Chatoorgoon (2007) used his non-linear code SPORTS (Chatoorgoon 1986) to study a system of parallel heated channels with supercritical water in a horizontal orientation. Non-dimensional parameters were derived using a point heat source model. A stability map was created to compare the numerical predictions of instability boundary with those of analytical instability boundaries calculated using the non-dimensional parameters. In addition to this, the threshold of supercritical flow instability of horizontal channels was found to be near the second derivative of the pressure drop versus mass flow rate curve. Moreover, he reported the accuracy of the state equation is important for predicting the correct onset of oscillation in a parallel channel system. Chatoorgoon (2013) assessed his new non-dimensional parameters for static instability analysis. His parameters are restricted to the flow instability boundary in supercritical parallel channels. These parameters might be useful for engineers as design tool as they can be used to asses flow stability in heated channels without the need for a formal stability analysis. Furthermore, this study also extends the use of new non-dimensional parameters for different flow orientations such as down-flow, up-flow, and horizontal flow. The stability analysis showed that vertical down-flow orientation was most susceptible to have static instability as compared to horizontal flow and vertical up-flow. Also, it was found that there exists a cut off temperature above which no static instability was found in up-flow. Non-dimensional parameters for oscillatory flow instability were also developed, and it was found that oscillatory instability can occur in down-flow, but at higher temperatures

Sharabi et al. (2009) performed transient 3-D stability analysis using CFD FLUENT code in simulating density wave oscillations. The physical model considered in this study was circular rod bundles with triangular and square pitch assemblies that are similar to the ones proposed for supercritical water fast reactor (SWFR) core. The inlet and outlet valve throttling were neglected. The results, however, provided an insight into the stability mechanism in triangular and square pitch rod bundles. The results concluded that density wave oscillation in the two geometries had similar characteristics as in circular channels.

Hou et al. (2011) used both time domain non-linear analysis and frequency domain 1-D analysis. They performed a detailed study of the newly proposed SCWR-M (mixed-spectrum core design) whose core design consists of two zones with different neutron spectrums (a thermal spectrum and a fast spectrum). This study mainly focused on the stability analysis of the fast spectrum. A simplified model of 3 parallel channels with inlets connected to a common inlet plenum and the outlet of the parallel channels connected to the outlet plena was used. Non-linear analysis verified a transitional stability region within the range of operating parameters for the fast spectrum. A stability map was also constructed and it verified that SCWR-M was stable under a wide range of operating conditions. In addition to this, different axial power distribution profiles were also analysed, which concluded that cosine-shaped or fork-shaped axial power distribution was more stable than uniform axial power shape. Finally, the comparison between linear and non-linear analysis yielded a good agreement in predicting the stability boundary of the system.

Xiong et al. (2012) experimentally studied supercritical H_2O instability in two heated vertical parallel channels. This was the first reported supercritical flow experimental study using H_2O. The total flow rate was driven by a pump. The test section of the loop was two INCONEL 625 tubes with a circular cross-section. The inner diameter and outer diameter of the tubes was 6 mm and 11

mm, respectively. A total of 9 instability boundary points were obtained. This study provided a great deal of insight on the dynamic characteristics of parallel channel instability. It also showed that before the onset of parallel channel instability, the flow rates in the two channels were quasi-symmetric at low fluid outlet temperatures and heat flux. As the heat flux increased, the fluid outlet temperatures reached near the pseudocritical temperatures and the flow in the two channels redistributed and became asymmetrical. At this point, the outlet fluid temperature of the channel, with lower flowrate, increased further. Another increase in heat flux lead to the irregular fluctuations of the two channels. However, the total flow rate remained constant. Finally, near the instability boundary, the two flow rates began to oscillate 180° out-of-phase. They concluded that the redistribution of flow rated between the channels played a vital role in the stability of the system. The redistribution of the flow rates in the experiments owed to the properties of supercritical water, especially the density of the fluid at the outlet. Furthermore, the parametric studies concluded that the stability of a system can be enhanced by increasing the system pressure or decreasing the inlet temperature.

The experimental investigation of Xiong et al. (2012) provided a great deal of understanding on the effect of system parameters on the instability boundary. However, the non-monotonic effect of inlet temperature was not verified due to the critical wall temperature limitation of the experimental facility. This non-monotonic effect of inlet temperature for a single heated channel with supercritical pressures was predicted by Ambrosini and Sharabi (2007). Xiong et al. (2013) did a non-linear analysis to verify the non-monotonic effect of inlet temperature. They modelled a simplified parallel channel system that was proposed in previous experimental study (Xiong et al., 2012). The code showed that increasing the inlet temperature degrades the stability of the system. However, there exists a point after which increasing the inlet temperature enhances the stability of

the system. This kind of non-monotonic effect of inlet temperature is well known for two-phase flow instabilities (Boure et al., 1973; Fukuda and Kobori, 1979).

Ampomah-Amoako et al. carried out series of studies using 3-D CFD code STAR-CCM+ and 1-D RELAP5 code to study flow stability in 3-D nuclear reactor sub-channels and 1-D heated channels with supercritical water (Ampomah-Amoako and Ambrosini, 2013; Ampomah-Amoako et al., 2013a, 2013b). The first part of the research was mainly focused on pure thermo-hydraulic flow instabilities. A CFD methodology was first developed, relatively coherent results of the periods of the oscillations and the stability threshold for different physical models confirmed the capabilities of the considered CFD code. It also suggested that the instability phenomenon of heated channels was mainly characterised by 1D behaviour. For the second part, vertical upward flow, vertical downward flow, horizontal flow were studied with both STAR-CCM+ and RELAP5 code. Decay ratio and period of oscillations of the two codes generally agreed well.

Su et al. (2013) used the non-linear time domain STAF code to investigate flow instability in a parallel channel system. The model simulated was two vertical parallel channels with inlet connected to an inlet plenum and the outlet of the channels connected to the outlet plenum. Supercritical water was used as the working fluid with constant mass flow simulating forced circulation. The study focused on the effect of flow parameters (total mass flow rate, system pressure, inlet temperature, heat flux, pressure drop and so on) and structural parameters (length of heated section, riser and entrance section, inside diameter and so on) on the stability of the system under consideration. The study concluded that the flow instability in two parallel channel system was similar to DWO. Flow pressure drop, the compressible volume of SCW (Super Critical Water), and the flow split between the two channels are the major factors, which excite the parallel channel instability. In addition to this, they concluded that increasing the mass flow rate, system

pressure or decreasing the heat flux enhances the stability of the parallel channel system. They also concluded that decreasing the inside diameter increases the stability of the system.

Debrah et al. (2013a) used 1-D RELAP5 system code and an in-house code, written in dimensionless form and based on the non-dimensional parameters of Ambrosini and Sharabi (2007), to study the stability of a natural circulation loop at supercritical pressure. The results showed the importance of heating structures. The study concluded that instability boundary predicted for the loop without heating structures were closer to the experimental values, whereas with the inclusion of the heating structures, the predicted instability boundary was way beyond the experimental boundary. In particular, the addition of heating structures stabilized the loop. Debrah et al. (2013b) carried out linear and non-linear analyses with reduced thermal capacitance of the wall. The results supported the finding of the previous study and it was recommended not to use heating structures in further thermal hydraulic stability analyses.

A 3-D simulation using the CFX code was performed by Xi et al. (2014a) to model the same loop geometry of Xiong et al. (2012). The purpose of this study was to analyze the oscillatory instability between two parallel channels with a 3-D code. Different turbulence models, mesh counts, coupling methods were used. Good agreement between 3-D simulation predictions and experimental results were reported. Finally, the results of 3-D simulation and 1-D simulation were compared to experimental results. They concluded that the effect of system parameters such as inlet mass flow rate, gravity, and system pressure on the onset of flow instability in CFX results was different from that obtained by 1-D code, especially gravity, which not only affected the instability power but also oscillation period. Also, they stated that the 3-D code can predict the onset of instability boundary better than 1-D code. However, the period of oscillation was overpredicted.

An independent 3-D study was performed with the CFX code by Li et al. (2016) to analyse further the results and conclusions made by Xiong et al. 2012, 2013; Xi et al., 2014a. Li et al, on the contrary, determined that conclusion of Xi et al. (2014a) were not accurate. The reason cited was the time step used by Xi et al., which was too large for accurately determining the stability boundary. Furthermore, non-linear 1-D SPORTS code (Chatoorgoon, 1986) predicted the stability boundary much better than the 3-D CFX simulations and the 1-D non-linear code of Xiong et al. (2013). The reason for this was stated to be the inlet and outlet pressure boundary conditions. Xiong et al. imposed static pressure boundary conditions at both inlet and outlet of the channels whereas, in SPORTS code simulations, equal stagnation pressure was imposed at inlet and outlet of the channels. Li et al also performed sensitivity studies, which concluded that time step size, number of iterations per time step, and the use of different transient scheme had great influence on prediction of stability boundary while the refinement of grid spatial size had negligible effect. Li et al concluded that first order transient scheme should be used in future investigations.

Liu et al. (2014) did a follow up study on the thermal spectrum zone of the SCWR-M. Liu et al. used a similar approach as used by Hou et al. (2011). 1-D linear and non-linear analyses were done to understand the stability of the thermal spectrum. The study concluded that wall thermal conductivity can degrade the stability of the system. However, if the value of wall thermal conductivity was high enough, the stability was not affected. Increasing the inlet mass flowrate enhanced the system stability. Frequency-domain model was used to generate stability maps, which showed a wide range of stable operating conditions.

Xi et al. (2014b) investigated oscillatory flow instability experimentally. The experimental set up used in this investigation was same as used in a previous study (Xiong et al., 2012) with some minor modifications. In the study by Xiong et al., the wall thickness of just 2.5 mm. As a result,

few stability data points were obtained. In this study, Xi et al. used a wall thickness of 6.5 mm. Also, the length of the heated channels (3105 mm) was divided into two sections using three copper plates arranged averagely along the axial direction. The section close to the inlet and outlet was called inlet section and outlet section respectively, and the power to each section was controlled independently to simulate different axial power distribution profiles. This was the first attempt to experimentally study the effect of non-uniform axial power distribution profile on supercrtical flow instability. Three different axial power distribution profiles were used; axially decreased, uniform, and axially increased power distribution. It was found that with axially decreased power distribution, the out-of-phase oscillation were observed three times. No out-of-phase oscillations were found with axially increased power shape. With the use of a uniform power shape, out-of-phase oscillation occurred at high heating flux. On comparing the three axial power distributions, uniform power distribution was determined to be the most stable power distribution profile. Finally, not only the inlet mass flow oscillated out-of-phase, but the outlet temperature also oscillated out-of-phase with the same time-period as the mass flowrate.

Non-linear analysis of parallel channel system was performed by Sharma et al. (2015) using the in-house NOLSTA-P code. The system studied was two vertical parallel channel closed loop with a tube-in-tube type cooler. The loop was a uniform diameter pipe with ID and OD 13.88 mm and 21.34 mm, respectively. The fluid used was H_2O, which was driven via natural circulation. The code was first used to simulate the experimental results obtained by Xiong et al. (2012) to verify the predictions of the NOLSTA-p code. The code predicted the instability boundary with a maximum deviation of 9.4 % from the experimental results.

Moreover, the code predicted a large unstable zone when the wall thermal energy storage effect was neglected. However, with the consideration of the wall thermal energy storage effect, the

system was completely stable. In addition to this, the equal/uniform power distribution was found to be more unstable than unequal/non-uniform power distribution.

Dutta et al. studied analytically the in-phase and out-of-phase DWO's in the CANDU supercritical water reactor concept (Dutta et al., 2015). A non-linear 1-D thermal-hydraulic code called THRUST was modified to model multiple parallel channels. The code was first validated with the experimental data of Xiong et al (2012). The code predictions agreed well with the experimental data with a maximum deviation of less than 5%. After this, the code was used to model and simulate the CANDU SCWR. The investigation on the in-phase DWO's concluded that as the asymmetry of power distribution between the parallel channels increases, the system becomes unstable. A Similar conclusion was made for the out-of-phase DWO's.

In addition to this, the effect of inlet loss coefficient was also investigated. The study showed that increasing the inlet k-factor enhances the system stability in case of both types of DWO's.

Ebrahimnia et al. (2016) used the CFD code ANSYS CFX v14.5 to study 2-D axisymmetric turbulent flow with supercritical water flowing up in a vertical pipe with constant applied wall heat flux. The RANS model was used to solve the governing equations. The static and oscillatory flow instabilities were analysed using the standard k-ϵ model with scalable wall-function and the k-ω-based SST model and the results were compared with the in-house 1-D SPORTS code (Chatoorgoon, 1986). Furthermore, the effect of changing the turbulent Prandtl number on the instability threshold was also examined. Results showed that threshold of instability predicted by the two turbulent models as well as the 1-D code agreed well. The effect of changing the turbulent Prandtl number on instability boundary had negligible effect.

Shitsi et al. conducted numerical investigations of flow instability using 3-D CFD code STAR-CCM+ (Shitsi et al., 2017). The model used was the experimental geometry of Xi et al., (2014b). The aim was to capture the out-of-phase oscillation and get insight on the effect of different system parameters on the amplitude and period of oscillation. The STAR-CCM+ code showed that the effect of system parameters does not affect the period of oscillations significantly. However, the amplitude of mass flow oscillation increased with increasing the heat flux. The system became more stable with constant axial power shape, as compared to the non-uniform axial power distribution. The system without the influence of gravity was more stable than that with the influence of gravity. The non-linear instability boundary predictions were close to the experimental results with maximum error of 10%, which proved that STAR-CCM+ code can predict the stability boundary and can capture the dynamic characteristics of the system.

Ghadge et al. (2018) used an in-house linear code (Chatoorgoon and Upadhye 2005) and the 3-D CFX code ANSYS and modeled Xiong et al. (2012) and Xi et al. (2014b) experimental cases. This study provided a great deal of understanding about the period of oscillation and the effect of wall thermal energy storage on the flow instability boundary. The study concluded that the inclusion of wall thermal energy storage can significantly affect the predicted single-channel stability, but there is a cancelling effect in the case of two identical parallel channels and the predicted instability boundary is unaffected by wall thermal energy storage effects. Moreover, the period of oscillation was predicted more accurately by including wall thermal energy storage effects. This was the first reported findings in open literature.

Singh and Singh (2019) performed a non linear analysis of a single inclined heated channel with CO_2 at supercritical conditions. They used a nodalized reduced order model (NROM). The study reports on the dynamic and static instabilities corresponding to different types of bifurcations.

Furthermore, parametric study concluded that increasing the inlet loss coefficient (K_{in}) enhances the stability of the system, whereas increasing the outlet loss coefficient (K_{out}) destabilises the system. The effect of inclination angle on the stability boundary is significant at high subcooling number where the gravitational pressure drop contributes significantly to the total pressure drop.

2.3 Summary

References	Type of study	Applications	Findings
Review of two-phase flow instabilities. (J.A. Boure et al.,1972)	Survey: Classification of different instabilities	Design parameters: mechanism of flow instabilities and analysis methods	1) Classification based on physical mechanism of two-phase flow instabilities 2) Clear distinction between "static" and "dynamic" instabilities and primary and secondary phenomenon has been proposed. 3) Analysis method of various types of two-phase flow instabilities has been reviewed.
Classification of two-phase flow instability by density wave oscillation model. (Fukuda et al., 1978)	Experimental: Test fluid: H_2O Pressure: 0.098 -6.86 MPa ΔT_{SUB}: 0-50°C Fluid flow: Natural circulation and Forced circulation. Analysis: Dynamic analysis	Design parameter: 1) Cause of flow instability based on transfer function. 2) Investigation of length of riser piping	1) Experimental investigation concluded two types of instability categorised as "Type I" and "Type II". The former was observed in a region having zero exit steam quality, and the latter occurs at high steam quality region. 2) Analytical study provided the basic transfer functions which are involved in the cause of instabilities mentioned in "1". In addition to this, classification of eight different types of instability based on different pressure drop terms is also done.
Forced convective heat transfer to supercritical water flowing in tubes (Yamagata,1971)	Experimental: Test fluid: H_2O Pressure:22.6-29.4 MPa T_{in}:230-540℃ Forced circulation	Heat transfer Correlation at supercritical conditions	1) At low heat fluxes, heat transfer coefficient (α) has a peak value, when bulk fluid temperature is slightly less than pseudocritical temperature. This peak value decreases as heat flux is increased or the pressure is increased.

			2) A correlation presented in this paper predicts 'α' better at low or moderate heat flux than other proposed correlations at the time. 3) A limiting value of heat flux above which heat transfer deterioration is significant for vertical up flow is found.
An analysis of thermally induced flow oscillations in near-critical and supercritical thermodynamic region (N. Zuber ,1966)	Theoretical analysis: system under investigation: flow through a heated duct at supercritical conditions.	Characteristic equations for different mechanism of flow instabilities under near-critical and supercritical conditions.	1) A method for analysing fundamental nature of periodic and aperiodic oscillation in supercritical flow was presented. The fluid domain was divided into two regions: 'heavy fluid region' and 'light fluid region'. The two regions separated by a transition point. 2) The difference in mechanism of two-phase flow instabilities and supercritical flow instabilities was also discussed.
Hot-channel stability of supercritical water-cooled reactor (Zhao et al., 2005)	Analytical: Linear perturbation and non-dimensional analysis	US. Reference SCWR Design. Steady state and sliding pressure start-up.	1) A three-region model: 'Heavy fluid region' with constant density, 'heavy and light fluid mixture region' and 'light fluid region' which is assumed as ideal gas. 2) Two non-dimensional parameters: 'Pseudo subcooling number' and 'expansion number' were found to be the governing parameters for single channel supercritical flow instability.
Dimensionless parameters in stability analysis of heated channels with fluids at supercritical pressures. (Ambrosini and Sharabi., 2007)	Analytical: Finite difference. RELAP5/MOD 3.3	SCLWR: stability analysis of heated channels using new derived parameters.	1) New non-dimensional parameters derived using critical point as the reference point. 2) Stability analysis of heated channel using finite element model and RELAP5/MOD3.3 proved the validation of the non- dimensional parameters. 3) Under some conditions, static Ledinegg instability was predicted.
Supercritical flow instability in parallel channels (Chatoorgoon V., 2007)	Analytical: Non-linear SPORTS code.	SCWR: Parallel channel instability boundary prediction.	1) Non-dimensional parameters governing parallel channel instability in horizontal channels. 2) Difference between two phase flow parallel channel instability and supercritical parallel channel instability.

			3) Accuracy of equation of state is found to of foremost importance in predicting flow instabilities in supercritical conditions.
Stability analysis of parallel-channel systems with forced flows under supercritical pressure. (Hou et al., 2011)	Analytical: Linear (frequency domain 1-D) Non-linear (time domain 1-D)	SCWR-M: which is a new core design having two zones fast zone and thermal zone. Stability of Fast-spectrum zone	1) Non-linear analysis verified a transitional stability region. 2) Stability maps generated through frequency domain analysis verified that under normal operation fast spectrum zone is stable. 3) Under unstable conditions, the hottest channel dominated the stability of parallel-channel system, i.e. the higher the power density of the hottest channel, the more unstable conditions the system experiences. 4) Non-linear and linear calculation shows a good agreement between the results.
Experimental study on flow instability in parallel channels with supercritical water. (Xiong et al., 2012)	Experimental: Fluid used: H_2O Pressure: 23-26 MPa. T_{in}= 180-260° C. Forced circulation: 600-800 kg/m^2 s.	SCWR- parallel channel flow instability with supercritical fluid. Comparison of mechanism of two-phase flow and supercritical flow instability.	1) Parametric study shows that the system becomes more stable with increase of system pressure and decreasing the inlet temperature. Two-phase flow instability phenomenon shows a similar trend. 2) This experimental study provides data for code validation, which is rare in this field.
Theoretical study on the flow instability of supercritical water in the parallel channels. (Su Y. et al., 2013)	Analytical: Non-linear 1-D code STAF	SCWR- flow instability in parallel channels.	1) Flow instability in supercritical conditions is excited by flow pressure drop, variation on the volume of SCW, distribution of mass flow between heated channels. 2) The shape of Marginal Stability Boundary (MSB) obtained at supercritical condition in this work is identical to MSB obtained under subcritical conditions suggesting the similarity of the two. 3) Stability of parallel channels is dominated by pressure drop. Moreover, parametric study concluded that increasing the mass flow and system pressure,

			decreasing the heat flux stabilises the parallel channel system.
Modeling and analysis of supercritical flow instability in parallel channels. (Xiong et al., 2013)	Analytical: Non-linear 1-D code developed in-house (SCIA).	SCWR- extending the parametric effects on parallel channel flow instability modeling techniques for experimental model used.	1) Analytical study showed good agreement with experimental results. 2) Effect of inlet temperature was found to be non-monotonic, which is well know for two phase flow instabilities concluding the mechanism of two-phase flow instabilities and supercritical flow instability are alike.
Discussion on the stability of natural circulation loops with supercritical pressure fluids. (Debrah et al., 2013a)	Analytical: 1-D-Linear 1-D-Non-linear	Natural Circulation Analysis of the CIAE natural circulation loop with supercritical water.	1) Without using wall heating structures, the results predicted were close to experimental results. 2) With the addition of wall structures the predicted results were way over the experimental results.
Assessment of a new model for the linear and nonlinear stability analysis of natural circulation loops with supercritical fluids. (Debrah et al., 2013b)	Analytical: 1-D-linear 1-D-Non-linear	Natural Circulation Reduced thermal capacitance of the wall was used in linear and non-linear analysis.	1) With the addition of wall heat structures and inclusion of wall heat transfer and friction correlations for normal fluids, the results were not satisfactory in comparison to experimental results.
Numerical simulation of flow instability between two heated parallel channels with supercritical water. (Xi et al., 2014)	Analytical: 3-D CFD simulation using Ansys CFX code.	SCWR- 3-D simulation of parallel channel instability. Effect of using different numerical models on instability boundary.	1) Parametric study concluded that influence of system pressure, inlet mass flow rate and gravity on the onset of flow instability is different obtained from that of 1-D code. 2) Using different numerical models have significant influence on flow instability analysis. 3) Prediction of instability boundary using 1-D code and 3-D code concerning experiments concluded that 3-D code predictions are more accurate.

An experimental investigation of flow instability between two heated parallel channels with supercritical water. (Xi et al.,2014)	Experimental: Fluid used: H_2O System pressure: 23-24 MPa. T_{in}= 180-260°C Forced circulation: M_t= 125 kg/h, 145 kg/h Uniform and non-uniform power distribution	SCWR: Experimental investigation of parallel channel instability. Influence of flow parameters, uniform and non- uniform power shapes on instability boundary.	1) Two types of out of phase oscillation were observed with time 'inlet mass flow rate' 'outlet temperature' with nearly same period. 2) The influence of uniform and non-uniform axial power shape concluded that system is more stable with uniform power. 3) Period of oscillation and amplitude are not sensitive to influence of total inlet mass flow rate, axial power shape and system pressure.
A supercritical pressure parallel channel natural circulation loop. (Sharma et al.,2015)	Analytical: Non-linear 1-D code NOLSTA-p	SCWR: stability analysis of parallel channels. Effects of including wall heat storage effects.	1) The code predicts large unstable zone for parallel channel loop without the wall heat storage effect. However, including the wall heat storage effect, the loop is completely stable.
Analysis of parallel channel instability in the CANDU supercritical water reactor. (Dutta et al.,2015)	Analytical: Non-linear 1-D code THRUST	CANDU SCWR: Stability of three parallel channels resembling the core of CANDU SCWR. Effect of asymmetrical heating power on the stability boundary. In-phase and out-of-phase DWO have been studied	1) Increasing asymmetrical heating power between parallel channels makes the reactor system less stable, specially with low enthalpy/temperature at inlet for both in-phase and out-of-phase DWO modes. 2) The effect of changing the inlet k-factor concluded that increasing the inlet k-factor enhances the MSB for both in-phase and out-of-phase DWO modes. However, the variation is very small.
Numerical stability analyses of upward flow of supercritical water in a vertical pipe (Ebrahimnia et al., 2016)	Analytical: Ansys CFX v14.5	Analyses of static and oscillatory flow instabilities using k-ϵ model with scalable wall-function and k-ω based SST model. Comparison of 1-D non-linear code predictions with CFD predictions	1) The results for instability threshold using k-ϵ and SST models were like 1-D results. 2) The k-ϵ model was recommended for stability predictions.

Numerical investigation of flow instability in parallel channels with supercritical water (Shitsi et al.,2017)	Analytical: STAR CCM+	SCWR: Dynamic characteristics of out-of-phase oscillations such as period and amplitude.	1) Results showed that amplitude of out-of-phase oscillations is significantly affected by system parameters. However, the system parameters do not affect the period of oscillation.
Numerical study of oscillatory flow instability in upward flow of supercritical water in two heated parallel channels (Li et al., 2018)	Analytical: Ansys CFX 3-D	Parallel channel instability: The effect of different turbulence schemes was studied on the prediction of stability boundary. The effect of changing the outlet plenum volume on the stability boundary was also analysed. Comparison of 1-D non-linear code with CFX 3-D code predictions	1) The study reviled that the use of first order transient scheme as opposed to second order transient scheme was much more reliable. 2) The comparison of 1-D code predictions and 3-D code predictions verified that 1-D code results were better than the 3-D results. 3) The effect of changing the outlet plenum volume had a negligible effect on the prediction of stability boundary.
Non-linear stability analysis for supercritical CO_2 flow in inclined heated channel (Singh and Singh, 2019)	Numerical: ROM model	Supercritical CO_2 flow: The effect of different parameters on the stability boundary and bifurcation points.	1) Several types of bifurcation are observed: Sub-critical and supercritical Hopf bifurcation, Generalized Hopf bifurcation, Bogdanov-Takens bifurcation. 2) Parametric study concluded that increasing K_{in} and/or decreasing the K_{out} enhances the system stability. The effect of inclination on the stability boundary is significant in the high sub-psuedo-critical number

Chapter 3 Experimental setup and Test procedure

3.1 Introduction

Recalling the previous chapter, it is evident that reported experimental data for supercritical flow parallel channel instability is sparse, compared to the literature for subcritical two-phase flow instability. To bridge this gap, an experimental flow facility named SFF-V was constructed at the University of Manitoba. The designing of this facility was done by Dr Vijay Chatoorgoon and was manufactured by Stern Laboratories. The facility was designed to capture the mass flow oscillation caused due to the feedback of flow rate and pressure drop, which is caused by the effect of large compressibility in the critical thermodynamic region. The new experimental facility is assembled in the Energy Lab at University of Manitoba. The facility consists of two loops: a primary and secondary loop. The details on the facility is provided in section 3.3. The following sections provide the details of the experimental facility and the test procedure.

3.2 Working Fluid: CO_2

Figure 3.1 shows the variation of thermo-physical properties of CO_2 above the critical point. The critical point of CO_2 corresponds to P_{cr} = 7.377 MPa and T_{cr} = 30.978 °C. This is lower than water (P_{cr} =22.064 MPa, T_{cr}= 373.95 °C). This was the main reason for using supercritical CO_2 instead of water. Additionally, the changes in thermophysical properties of CO_2 above the critical point show a similar trend when compared to water (Figure 1.5).

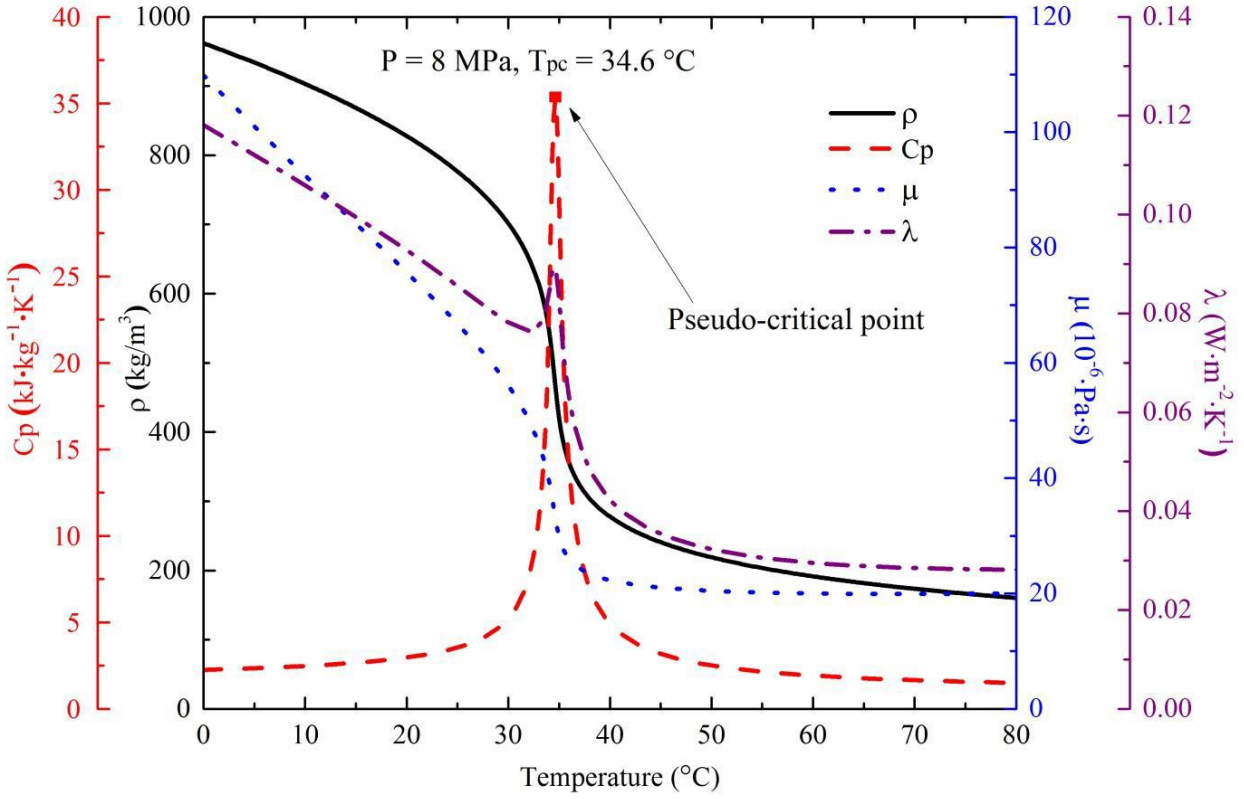

Figure 3.1: Thermo-physical property variation of CO2 at P= 8 [MPa]

3.3 Experimental Facility: SFF-V

Figure 3.2 shows the schematic representation of SFF-V. The SFF-V consists of a primary loop (working fluid: CO_2), and a secondary loop (working fluid: Propylene glycol and water solution). The primary loop (shown in figure 3.3) consists of a CO_2 gas booster, pressurizer, turbine flow meters, mixing plena, entry section, riser section, heat exchanger, ball valves, pressure relief valves and the test section, which is two vertical parallel channels. Each channel is connected to the inlet header with an entry section and the outlet header with a riser section. A turbine flow meter was installed on the inlet of each entry section. Two ball valves were also installed one at the inlet and one at the outlet of each channel. Additionally, a plate type heat exchange was installed to remove the heat from the working fluid. The facility was designed to sustain a maximum pressure of 15 MPa with safety release valves attached on the loop. If the maximum pressure goes above, 15

MPa, the safety release valves would open and release the excess pressure to the atmosphere. Details on the control systems and components are explained in the next section.

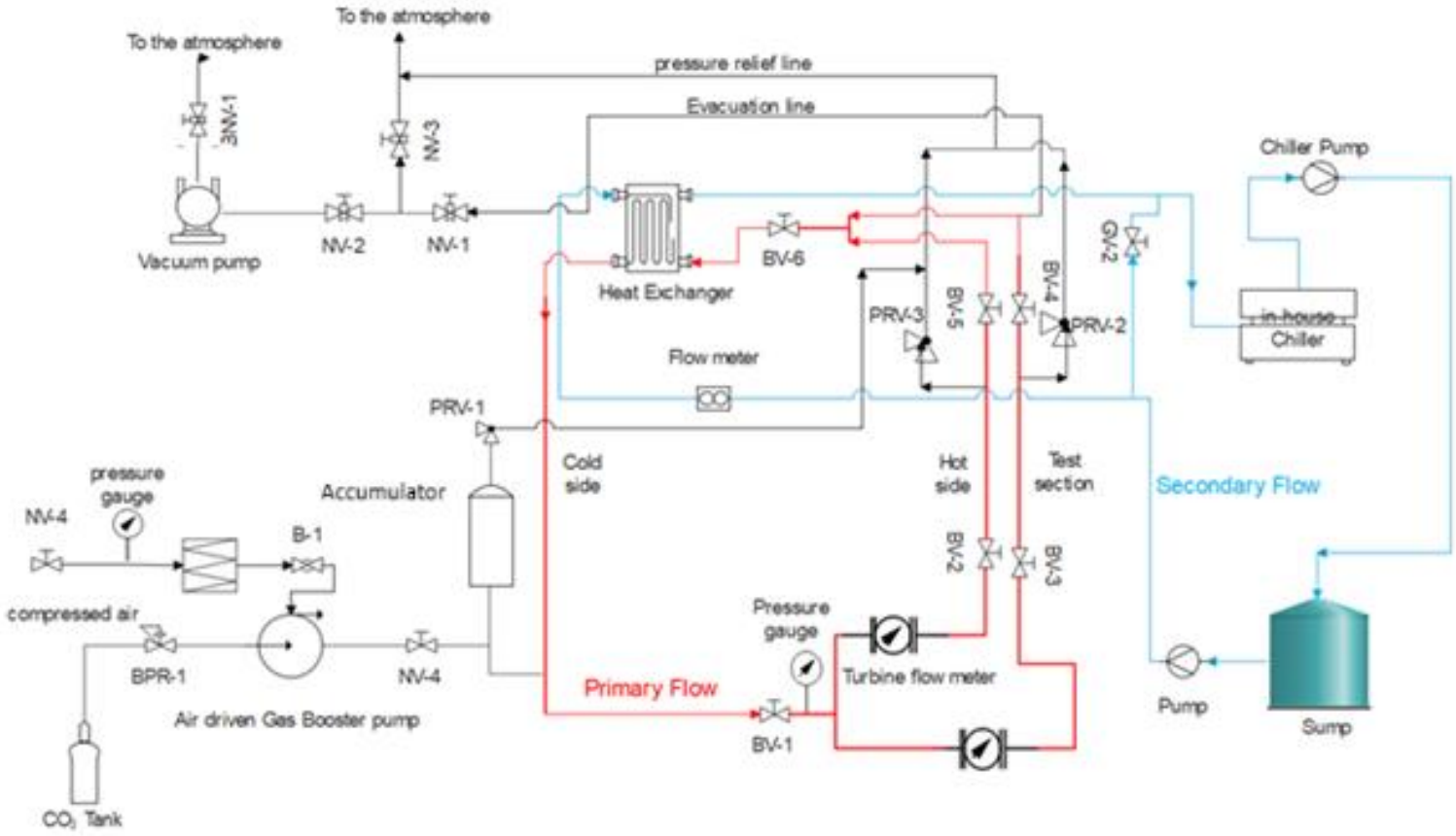

Figure 3.2: Schematic of experimental flow facility SFF-V

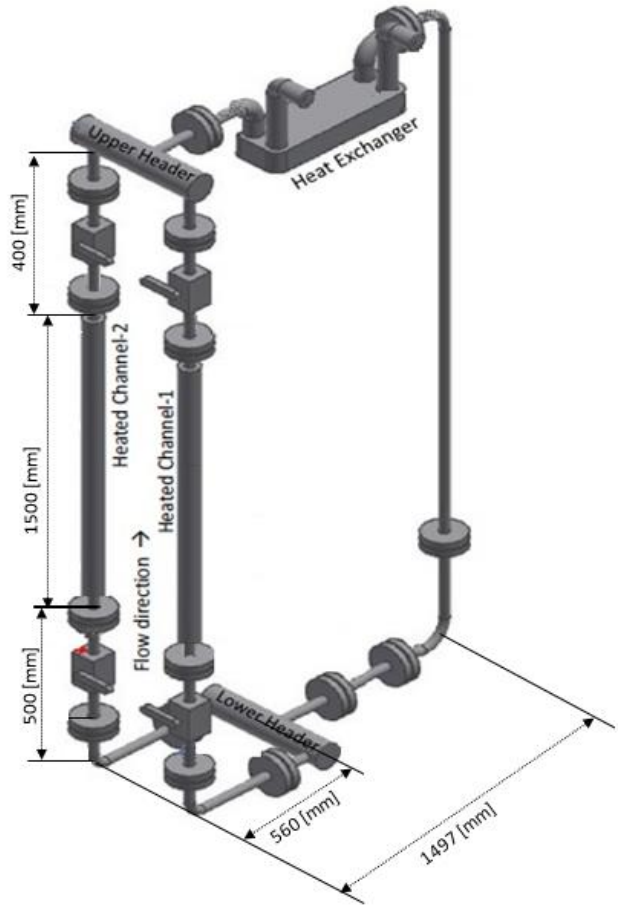

Figure 3.3: Detailed dimensions of the Primary loop (SFF-V)

3.3.1 Test section.

The test section of the SFF-V consisted of two vertical parallel heated channels made from INCONEL 825 seamless tubes with OD and ID 19.50 mm and 16.56 mm, respectively. The heated length of each channel was 1500 mm. The reason to use INCONEL as the material for the heated channels was to ensure that the heat flux along the axial direction was uniform since the change in resistance of INCONEL with temperature is minimal. The vertical channels were ganged by an inlet and outlet header. Figure 3.4 represents the test section.

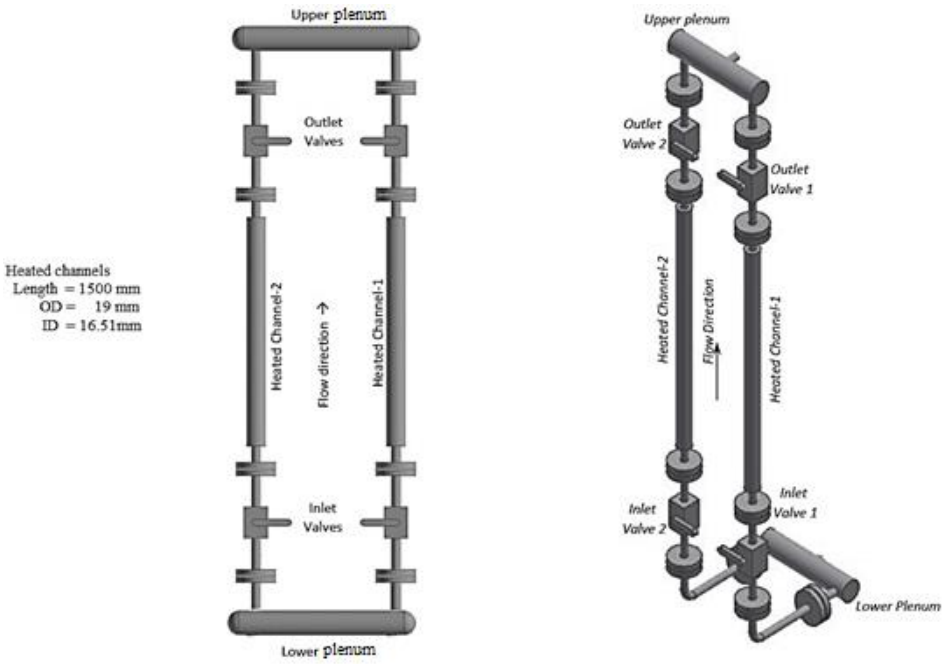

Figure 3.4: The test section

3.3.2 Pressure control system

Originally, the pressure control system consisted of Helium gas cylinder, check valve, single stage pressure regulator, accumulator, a back-pressure regulator and a glass fitted containment unit connected to the accumulator. The idea was to use gravity to cause the lighter He gas to stay at the top of accumulator and the heavier CO_2 to stay at the bottom. The He gas will either push down the CO_2, in case of a pressure drop in the system, or will raise the CO_2 level, if the system pressure increased.

3.3.2.1 Accumulator

Before performing tests, the pressure control system was tested. The back-pressure regulator was set at a predetermined operating pressure condition of 7.8 MPa. CO_2 was charged into the loop directly from the CO_2 cylinder; then the gas booster was used to increase the loop pressure to 7.6 MPa, then He gas was pumped into the accumulator to increase the system pressure to 7.8 MPa.

The liquid CO_2 and He gas interface could be seen in the glass containment. At this point, the temperature at the inlet increased and the secondary side cooling system was used to bring the temperature down to operating conditions. As the temperature was reduced, the pressure reduced and the interface between the liquid CO_2 and He gas was not observed. It was thought that all the liquid CO_2 was pushed into the loop and only He gas was in the accumulator. The heating power was increased, increasing the pressure inside the loop, and the interface was visible again. However, with a small increase of power, the channel wall temperature rose to about 500 °C, and the test was shut down. Some of the He gas had escaped into the loop because of the small volume of the accumulator. This was a big issue as it could jeopardise the purity of CO_2 and, hence, the test results. Finally, it was decided not to use He gas to regulate the pressure in the loop. Instead, the CO_2 was exhausted manually when it was required to reduce the loop pressure. Two needle valves NV-1 and NV-3 were used to release the excess pressure instead of the back-pressure regulator. This was the most effective and cost-efficient way instead of buying a new larger volume accumulator and He gas cylinder.

3.3.3 Pressurization system

The pressurization system was used to pressurize the loop to desired supercritical pressure. The main components of the system included a CO_2 tank (99.99% purity), and a gas booster.

3.3.4 Power supply system.

Electrical power was supplied to the test section from a 30-kW DC power supply (EMHP Power Supply), donated by Atomic Energy of Canada Limited (AECL), now known as Canadian Nuclear Laboratories (CNL). The channels acted as a resistive load and heated up as the electrical power was increased. A circuit breaker rated at 1500 Amps was installed between the rectifier and the test section. The power supplied to the test section was controlled via a LabVIEW software. The

scroll wheel of the mouse was programmed to increase or decrease the electrical power supplied by the DC power supply (Kalsi 2017).

It was found during a pre-test phase that the power supply, though rated to supply 30 kW, would shut down unexpectedly before 30 kW output was reached. The reasons for this was unknown, and after some study by this researcher and communications with the manufacturer, it was found that a jump connection was missing between 13 and 14 input connectors of the power supply, which was essential for the proper working of the power supply.

3.3.5 Vacuum and evacuation system

For accurate instability measurements, the purity of the working fluid is of utmost important as minute particle of air inside the loop can significantly affect the results. So, it was necessary first to vacuum the entire loop which was done with the help of a vacuuming system. The system included a vacuum pump and ball valves.

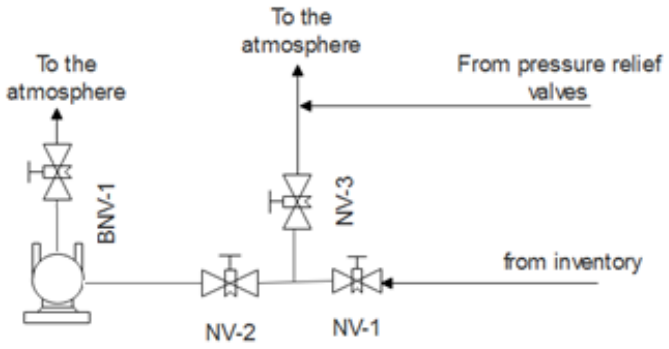

Figure 3.5: Evacuation system layout

3.3.6 Cooling system

One of two cooling systems was used depending on the weather, during the summer the in-house chiller was used, and during winter the roof top chiller was used as it is most effective in the winter time. Figure 3.6 and 3.7 shows the schematic of the two cooling systems used. On comparison,

though both the cooling systems share the same components, only one main difference exists. The first setup used an in-house air-cooled chiller unit (International Cooling Company) as the sink. This setup was mostly used in the summer to get inlet temperature down to 9° C. The rated capacity of the in-house chiller was 26 kW. The second setup utilizes a blower and cold weather outside as the heat sink. This setup is more powerful than the in-house chiller setup as it can remove up to 150 kW of heat depending upon the ambient temperature outside. The working fluid for both the setup was selected as Propylene glycol and water solution. More details can be found in Uddin (2015).

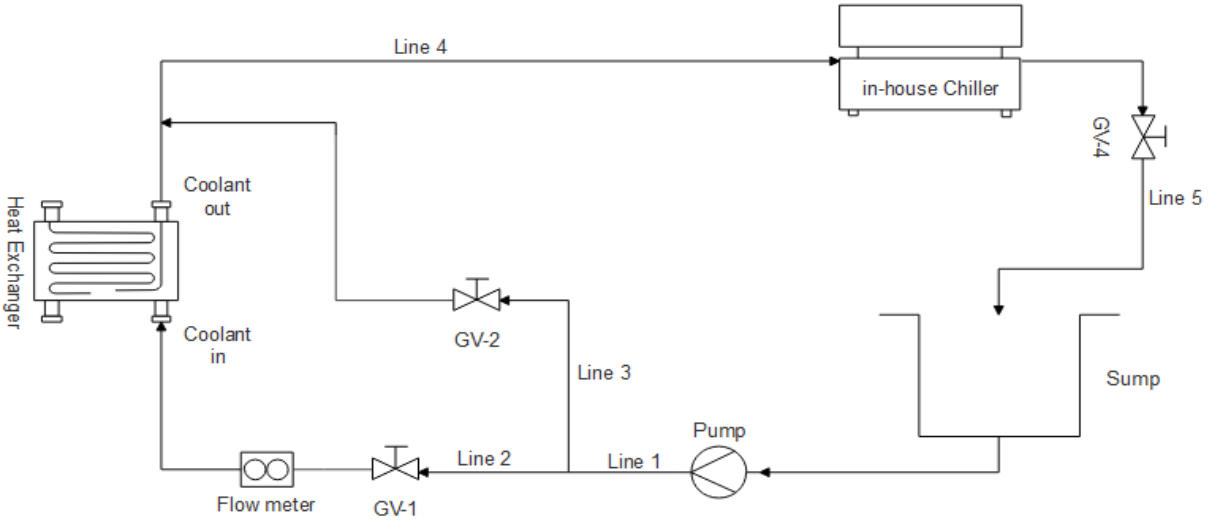

Figure 3.6: Cooling system with in-house chiller configuration

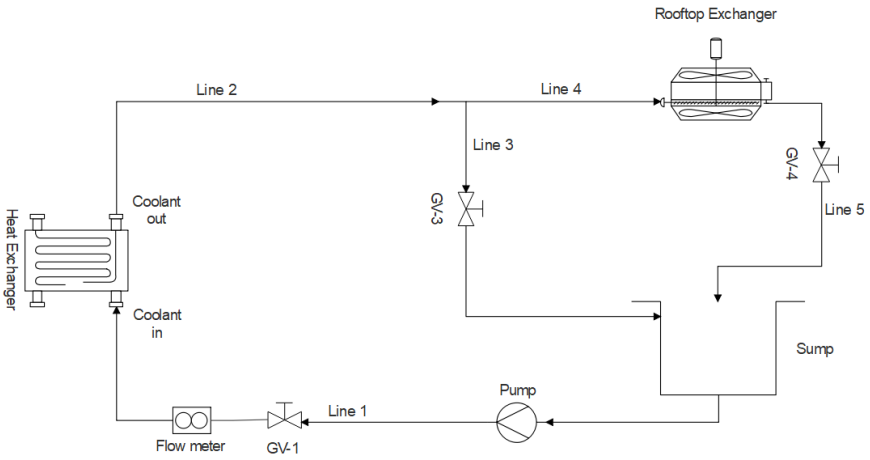

Figure 3.7: Cooling system with rooftop chiller configuration

The working of the two setups was also different. For the setup shown in figure 3.6, to control the CO_2 inlet temperature, the electronic panel with temperature controls on the in-house chiller could be set to the desire inlet temperature and the chiller would start extracting heat from the primary fluid when the temperature of the fluid rose above 1° C more than the pre-set temperature. The chiller continues to extract heat from the primary fluid until the temperature was 1 °C less than the pre-set temperature. Whereas, to regulate the inlet temperature of supercritical CO_2 with setup shown in figure 3.7, the mass flow rate of the coolant fluid was controlled with the help of a gate valve (GV-4) [Later replaced by a needle valve for better control].

3.3.7 Data Acquisition System (DAS)

Data acquisition (DAQ) is the process of collecting electrical or physical phenomenon such as voltage, current, temperature, pressure or sound. The process involves capturing a real-time condition and converting the resulting electrical signals into digital numeric values that can be processed by a computer. The main components of a DAS are sensors, signals, signal conditioning, DAQ module and a computer with software to read the digital numerical data. Figure 3.8 shows a simple block diagram of a DAS. In the current study, several sensors were used to measure real-

time physical conditions such as system pressure, wall temperature, primary fluid temperature, secondary loop coolant temperature, channel differential pressure, mass flow rate, and electrical power. Further details are provided in the instrumentation section.

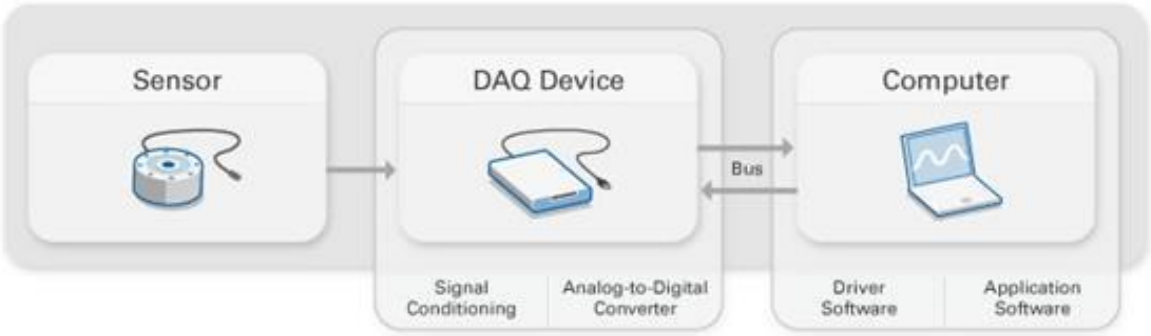

Figure 3.8: Block diagram of a DAS

3.4 Safety feature of SFF-V

Safe working is an essential part of our work environment. The current facility has many features that enhances safety. Some of the features were related to the hardware and some were programmed into the software used.

Figure 3.9: Safety features of SFF-V (in picture: Perspex glass enclosure, safety key and emergency stop button)

To make the facility blast proof, the whole experimental facility was contained in a Perspex containment. The doors of the Perspex containment are fitted with limit switches, which serves as a key. If during operation any of the two doors are accidently opened, the circuit would break and the power would shut down immediately.

A fail-safe key and lock system were also installed. If the key was in the lock and turned ON, only then the power supply will turn ON. Otherwise, no power will be supplied to the loop. If during operation there was a complication, an emergency stop button which when pressed immediately shuts down the facility. Figure 3.9 shows some the safety feature of SFF-V.

Pressure safety relief valves were also installed on the loop, which become active and release pressure when the system pressure rises above 11.38 MPa. In addition, programming in LabVIEW software also stops an experiment if the system pressure exceeds 10.34 MPa and\or the wall temperature exceeded 450 °C.

3.5 Instrumentations

To record different flow conditions and system parameters, various instruments were used. The parameters recorded were: system pressure, pressure drops, CO_2 volume flow rate, coolant flow rate, primary and secondary fluid temperature, wall temperature of test section, voltage drop across test section. Table 3:1 shows the summary of instruments used.

Table 3:1: Installed instrumentation on SFF-B for measuring different parameters

Instrument	Details	Purpose
Thermocouple	OMEGA Engineering Model: T-type, 1/8” sheath diameter	Fluid temperature measurement
Thermocouple	OMEGA Engineering Model: K-type, 1/8” sheath diameter	Wall temperature of the test section

Absolute pressure transducer	Validyne Engineering Corporation Range: 0-1500 psi	Absolute pressure measurement of fluid contained in loop
Differential Pressure Transducer	Validyne Engineering Corporation Model: P55 Range: 0-0.5 Psi	Pressure drop measurement across heat exchanger
Differential Pressure Transducer	Validyne Engineering Corporation Model: P55 Range: 0-0.5 Psi	Pressure drop measurement across valves
Differential Pressure Transducer	Validyne Engineering Corporation Model: DP303 Range: 0-8 Psi	Pressure drop measurement across heating channel
Turbine Flow Meter	OMEGA Engineering Model: FTB-1421 Range: 0.6~3 GPM	Supercritical CO_2 volumetric flow rate measurement
Turbine Flow Meter	Seametrics Model: SPX-050 Range: 0.6 ~ 40 GPM, 0.4 ~ 20 GPM, 0.1~10 GPM	Coolant volumetric flow rate measurement
Isolated DC Voltmeter	Wilkerson Instrument Corporation Model: SR2101 Range: 0 ~ 20 V	Measuring voltage drop across test section
Dial pressure gauge	Swagelok Pressure Gauge Range: 0~1500 psi	System pressure measurement.

3.5.1 Temperature measurement

Figure 3.10 shows the placement of thermocouples in the loop. A total of 20 thermocouples were placed to measure wall and fluid temperatures at different locations. Ten K-Type thermocouple

were used to measure the wall temperature of the two channels at five axial location. K-type thermocouples have an accuracy of ± 1 °C and have a wide temperature range of -200 to +1350 °C. Eight T-type thermocouples were used to measure the primary fluid temperature at the inlet and outlet of the heated channels, heat exchanger (CO_2 side) and at the inlet plenum and outlet plenum. Two additional T-type thermocouples were used to measure temperature of the coolant at the inlet and outlet of the plate type heat exchanger.

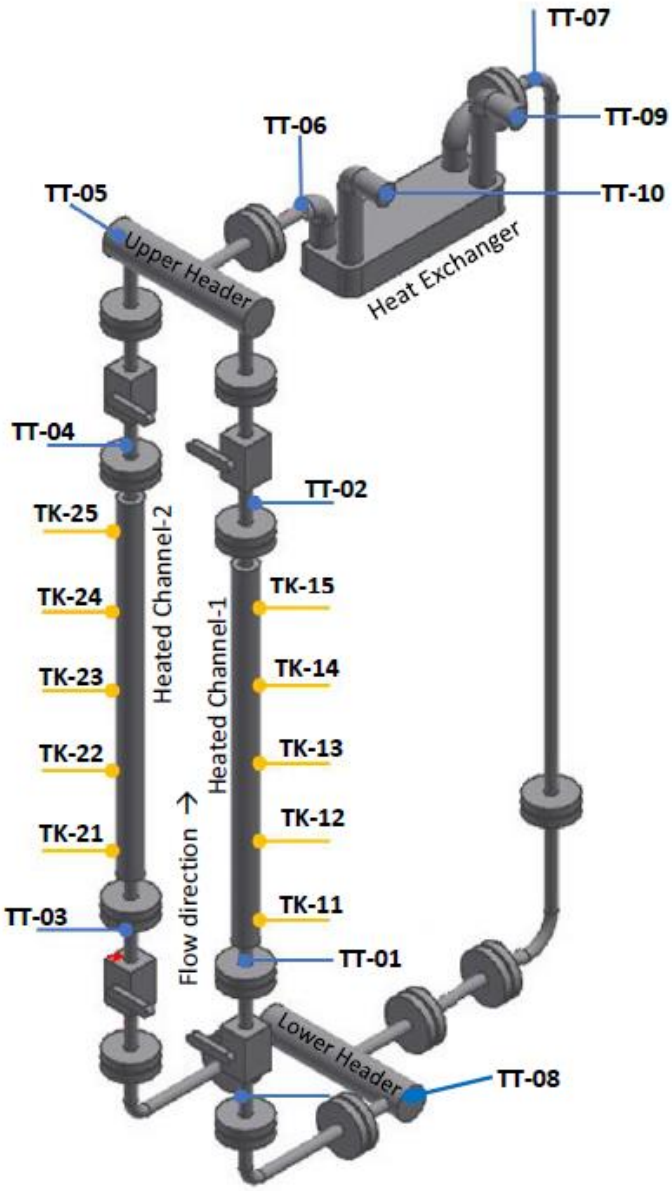

Figure 3.10: Placement of Thermocouples on the experimental facility.

3.5.2 Pressure and pressure-drop measurement.

For measuring the loop system pressure, an absolute pressure transducer of range 0 to 1500 psi (0-10.34 MPa) was attached at the inlet plenum. In addition to this, an analog (dial) pressure gauge of similar pressure range was also installed at the inlet plenum.

For pressure drop measurement, seven differential pressure transduces were used to measure pressure difference across the inlet and outlet channel valves, heated channels and heat exchanger. Figure 3.11 shows the placement of the eight pressure transducers. The differential pressure transducers are excellent for measuring dynamic signal with its fast response time (0.05 s) and accuracy (0.5% F.S. accuracy). The pressure transducers were calibrated to show voltage output when certain pressure drop was imposed. The details on calibration can be found in Kalsi (2017).

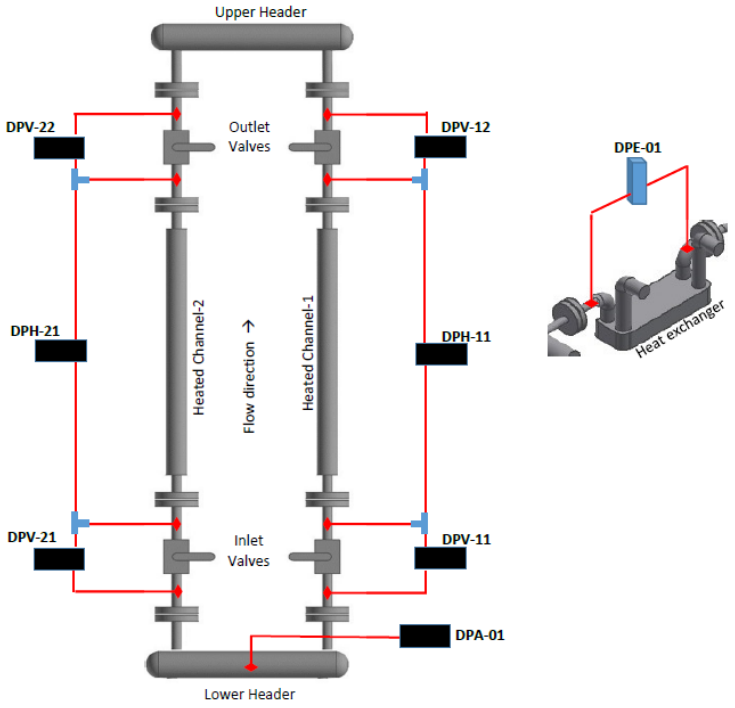

Figure 3.11: Location of pressure transducers on the experimental facility.

3.5.3 Flow measurement

To measure the flow rate of the primary fluid and the coolant, three flow meters were used. Two turbine flow meters were installed at the channels' inlet just after the inlet header to measure the primary volumetric flow rate of CO_2. And, one turbine flowmeter was used to measure secondary flow rate. The vanes of the turbine flow meters rotate at a speed proportional to fluid velocity. The rotation of the vanes was converted into A.C. pulses and were shown on a digital rate meter. The frequency of the rotating vane was used to calculate the volumetric flow rate of CO_2 using the following equation.

$$LPM = \frac{Hz * 60}{NK} \quad (1)$$

Where NK is the nominal flow meter K-factor provided by the manufacturer, LPM is the volumetric flow rate (liters per minute), and Hz is the frequency of the rotating vane.

Similarly, the pulses from the turbine flow meter on the coolant side were converted into digital output using another digital rate meter. An additional float meter was used to precisely control the coolant flow rate when using coolant system setup 2 (Refer: Figure 3.7: Cooling system with rooftop chiller configuration).

3.5.4 Electrical power and Heating power

The electrical power supplied to the test section was converted into heat due to the electrical resistance of the test section. However, due to losses, some electrical power was lost as heat loss to surroundings. Two isolated DC wire transmitter were used to measure the voltage drop across the two heated channels. The electrical power of the system was calculated using equation (2)

$$P = \frac{V^2}{R} \quad (2)$$

Where; P is the electrical power [W], V is the voltage drop across the heated channels [volts], and R is the resistance of the INC 825 test section [Ω].

The heating power, on the other hand, was calculated using the inlet and outlet enthalpy of the channel fluid with the know mass flow rate using equation (3).

$$Q = m(h_2 - h_1) \quad (3)$$

Where: Q is the heating power [kW], m is the mass flow rate [kg/s], and h_2 and h_1 are enthalpy [kJ/kg] of the fluid at outlet and inlet, respectively.

3.6 Uncertainty in measurement

Uncertainty is a measure of the inaccuracy contained in a measurement, and this inaccuracy can depend on a number of factors, such as small manufacturing defects in an instrument, uncertainty due to assumptions and human error. All this will lead to a measurement that is the measured value ± uncertainty. To explain this in simple words, taking an example of the current study, we use thermocouples to measure the fluid and wall temperature. However, the thermocouple is sold with an uncertainty of ± 1 °C. Many instruments were used in recording different parameters in the current experimental study and the uncertainty associated to those parameters are listed below and are summarised in table 3.2

3.6.1 Volumetric flow rate

The volumetric flow rate at the inlet of each entry section was measured by an FTB-1421 turbine flow meter. The meter accuracy, based on the calibration report provided by the manufacturer, is ± 0.72% for the upper 70% range and increases up to 1.68% for the lower 30% range. The maximum volumetric flow rate measured for all the cases here is in the range of less than 30%.

So, considering the different temperatures of CO_2 with respect to the ambient temperature of water used for calibration, an uncertainty of ± 2% was used for flow measurement.

3.6.2 Temperature measurement.

T-type and K-type thermocouples were used to measure the fluid temperature and wall temperature, as described in section 3.5.1. The T-type thermocouples have an accuracy of ±0.5° C, where as the K-type thermocouple have an accuracy of ± 1° C. However, an assumption was made here. The T-type thermocouples was placed at the center of the pipe, and the fluid temperature at the center was assumed to be equal to the area average bulk fluid temperature of the pipe. We know this would not be true. Similarly, the K-type thermocouples were brazed onto the outer wall of the heated channels and were assumed to be perfectly touching the wall.

3.6.3 Electrical power to test section

The electrical power was calculated using equation (2). The voltage drop across each heated channel was obtained by an isolated DC voltmeter, with an accuracy of ± 1% of the total span, and the resistance of the INCONEL channel was calculated based on the electrical resistivity variation with temperature. The temperature variation range selected was 25 °C to 400 °C. The temperature averaged calculated resistance was 0.255 Ω. The maximum uncertainty in measuring electrical power was 2.2%

3.6.4 Pressure measurement.

The pressure drop was measured with two types of pressure transducers: the DP55 and DP303. The DP 55 transducers were used to measure pressure drop across the inlet and outlet valves, and the DP303 transducer was used to measure the pressure drop across the heated channel. Kalsi (2017) calibrated the DP cells and the maximum error calculated was ± 4 %. The system pressure

was measured by an absolute pressure transducer, which was calibrated by the manufacturer and has an uncertainty of 0.5 %.

3.6.5 Heating power.

The heating power or the power to flow was calculated using equation (3) for every experimental case. A maximum uncertainty of ± 4.90 % was obtained.

Table 3:2: Uncertainty in measurement

Parameter	Uncertainty
Flow measurement	± 2 %
Fluid Temperature measurement	± 0.5 °C
Wall temperature measurement	± 1 °C
Electrical Power to Test Section	± 2.2 %
Pressure drop measurement	± 4 %
Pressure measurement	±0.5 %
Power to flow	±4.90%

3.7 Steps in preparing loop for pressurization

Before preforming any tests on the experimental facility, it was essential to ensure that all the measuring instruments and control systems work properly. To ensure this, certain tests were conducted and some measuring devices recalibrated to get accurate data.

3.7.1 Calibration

Calibration is the process by which the sensor electrical signal is adjusted so that it has a known relationship to the applied pressure. The differential pressure transducers were calibrated by using a pressure calibrator. The calibrator was first attached to the + ve end and – ve end of the DP cell and the values of ‘zero’ and ‘span’ were set. With ‘zero’ adjusted, the electrical signal of the DP

cell sends a 0 Vdc output signal when zero pressure was applied. Similarly, with 'span' adjusted, the DP cell sends an output signal of +10 Vdc when full span pressure was applied. More information on calibration can be found in Kalsi (2017)

3.7.2 Leakage testing

After doing the reinstallation of the pressure transducers and calibration was completed, the loop was tested for leaks. This test was performed by pressurizing the loop with CO_2 at 3.4 -3.8 MPa. The loop was left undisturbed for 30 minutes and the pressure in the loop was noted. Then the loop was left undisturbed for one day. If the pressure dropped significantly (say 0.8- 1.0 MPa), then the loop was sprayed with soap solution, usually on the reinstalled DP cells and on valves and fittings. With soapy solution, bubbles start forming if CO_2 was leaking from the sprayed spot. If the pressure drop was negligible, then the loop was boosted up to supercritical pressure and further examined for leaks.

3.7.3 Purging

The purging of the loop was done to flush out all air particles. The purging process started with opening all the valves on the primary loop, the needle valve NV-4, which was the inlet to the primary loop, and the two needle valves NV-1 and NV-3, which were the exhaust valves. The CO_2 supply was then opened to supply a burst of pure CO_2 four to five times in intervals of 5 minutes between each flush or burst.

3.7.4 Vacuuming

After successful leakage test and purging of the system, evacuation of the loop was done. CO_2 was slowly released to the atmosphere through the evacuation system. Slow leaking of CO_2 ensured that the DP cells did not get damaged and helped in removal of any air particles. After the loop was evacuated, the needle valves of the DP cells were closed. The valve NV-3 was closed and

valve NV-2 was opened simultaneously powering the vacuum pump. Vacuuming of the loop was done in intervals of 3 hours with 20 minutes of rest for the vacuum pump to cool down. A total of 12 hours of vacuuming was thought to be enough according to the loop piping volume. At the end of this step, the needle valves of the DP cells were opened.

3.8 Pressurization

Pressurisation of the loop begins with directly charging the loop from a CO_2 cylinder that supplied a pressure of 5.8 MPa. This raised the pressure of the loop to a pressure that was still subcritical. A gas booster with a compression ration of 20:1, capable of generating a pressure of 31.30 MPa, was used to increase the system pressure to the desired supercritical working conditions. Care must be taken here as the booster pump and the hose connecting the pump and the loop gets hot, which raises the CO_2 temperature and increases the loop pressure rapidly. This can damage the thin membrane of the DP cells. A rest of 15 minutes was adequate to let the pump and hose cool down.

3.9 Test Procedure.

After pressurizing, the loop was left undisturbed for 30 minutes for the CO_2 pressure and temperature to equilibrate. The outlet valves were adjusted to a predetermined position. Before doing an experiment, all instrument signals were checked to ensure proper working order. The following procedure was used:

1.) The in-house chiller was turned on to supply the secondary side coolant and achieve the desired inlet temperature of CO_2. As the CO_2 was cooled the system pressure decreased.
2.) A little amount of power was supplied to the test section (0.5-0.7 kW), which heated the CO_2 and raised the system pressure. Power was increased by 1 kW over 15 minutes until the pressure increased to the desired test conditions. Simultaneously, the secondary side

coolant flow rate was adjusted through a valve on the secondary loop to maintain the desired inlet CO_2 temperature.

3.) When the desired pressure and inlet temperature were achieved, data was recorded for initial conditions of the test for 5 minutes and then turned off.

4.) After this stage, the heating power was gradually supplied to the test sections in steps of 0.5 kW. At this point, the flow was already established in the loop.

5.) Steps 4 was repeated until instability or flow oscillation was observed. Only out-of-phase oscillations were sought.

6.) On observation of out-of-phase oscillations, the heating power was reduced by 1 kW to suppress the oscillations and data recording was started. The power was again increased, but with a smaller increment of 0.2 kW over 5 minutes to record data at the onset of instability. This data was later analysed to obtain the instability boundary mass flow rate and power.

Chapter 4 Experimental results

4.1 Introduction

In this chapter, the experimental results on flow instability at supercritical conditions in two vertical parallel channels are presented and discussed. This is the first reported experimental study on supercritical flow instability in two vertical parallel heated channels using CO_2, as previous experimental study was done with H_2O (Xiong et al., 2012; Xi et al., 2014b).

A total of sixteen cases were done with a range of inlet temperatures, system pressures, mass flow rates and various outlet k-factors. This data would be useful for validation and licensing of commercial codes.

The results presented herein were obtained using the procedure explained in chapter 3. This chapter explains how the onset of instability was determined, the onset of instability, the inlet flow phasing and the ensuing conclusions.

Additionally, the CO_2 data were converted to H_2O data using the non-dimensional parameters of Ambrosini and Sarabi (2007), which was then used to predict instability boundary using CATHENA code v3.5.4.4, as it can only model water.

4.2 Determination of Onset of Instability

Determination of the onset of instability was the objective of this study. Following method was employed in the current study.

The onset of instability was determined to occur when the channel inlet mass flow rate achieved sustained out-of-phase oscillation accompanied with evident amplitude enlargement. Figure 4.1 shows the onset of instability.

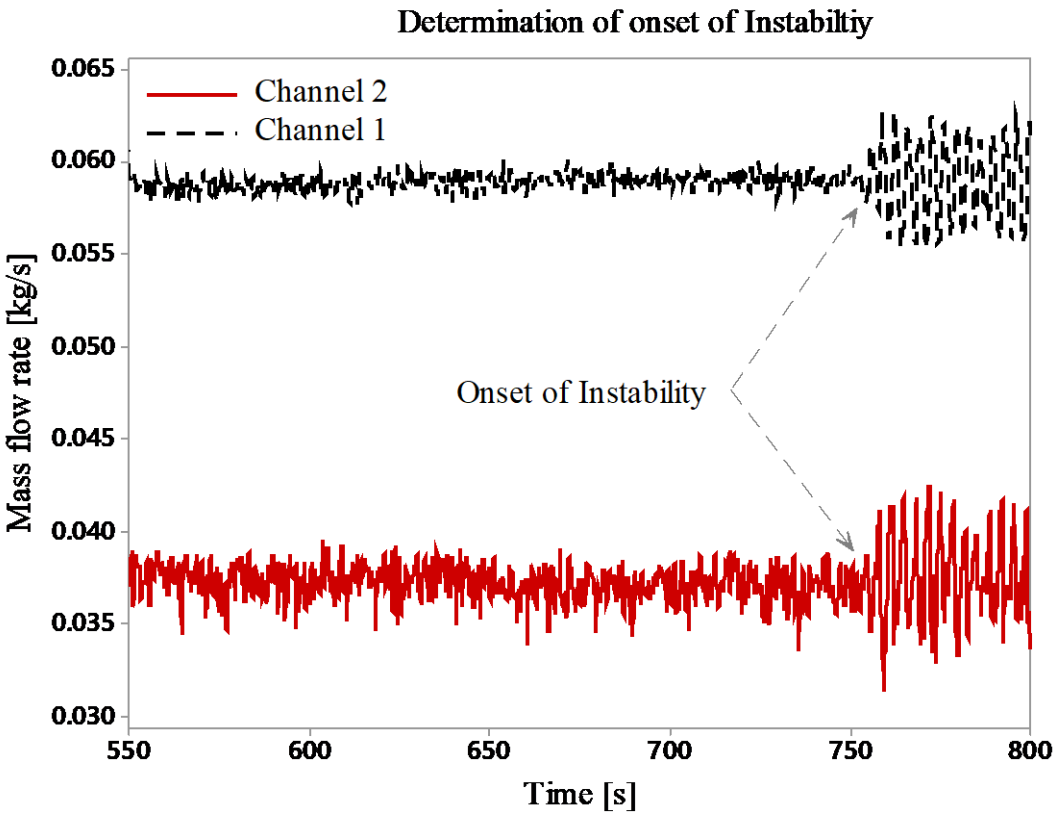

Figure 4.1: Onset of instability (Case 6)

4.3 Stability boundary Analysis

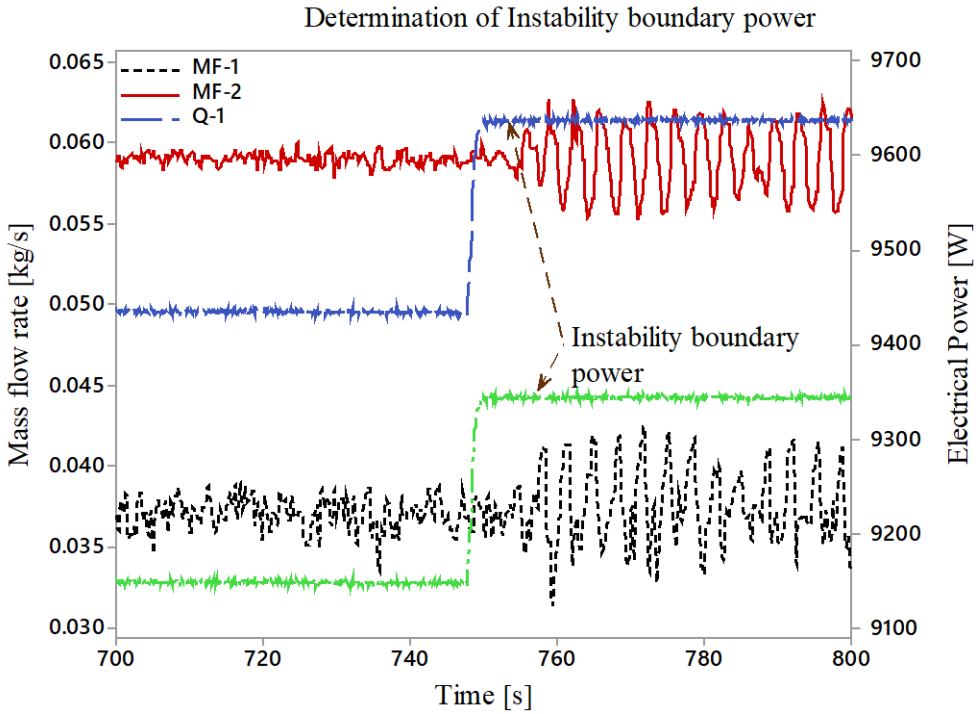

Figure 4.2: Instability boundary power

The recorded data, shown in the figure 4.1, were analysed to determine the stability boundary power and mass flow rate, as follows:

1) The recorded data, before the onset of instability was averaged to get the mean stability boundary mass flow rate.
2) To obtain the instability boundary power from the recorded data and get the time around which the flow starts to oscillate out-of-phase, the data was plotted as shown in figure 4.2
3) From the plotted experimental data, the instability boundary power was determined visually from the instability plot, which shows when the amplitude suddenly increased while the two channels oscillated out-of-phase.

Table 4:1: Parameters corresponding to stability boundary

Case No.	Power [kW]		Total flow rate	Channel flow rates [kg/s]	Inlet temp.	Outlet valve K-factor	System pressure	Period of oscillations [Seconds]
	Ch 1	Ch 2	[kg/s]	Ch1/Ch2	°C	Ch1/Ch2	MPa	Major/Minor
1.)	6.75	6.55	0.0938	0.0473/0.0465	15.80	5.2/5.8	7.4	1.0/11
2.)	10.43	10.13	0.0638	0.0347/0.0291	13.80	3.8/7.0	7.9	3.2/1.7
3.)	12.8	12.5	0.1227	0.0661/0.0566	15.85	4.6/7.2	7.7	3.4/1.6
4.)	9.12	8.85	0.1111	0.0578/0.0533	17.75	4.3/5.7	8.2	3.5/1.7
5.)	9.63	9.34	0.0962	0.0373/0.0589	17.25	13.0/2.2	8.6	3.2/1.6
6.)	9.42	9.13	0.0919	0.0356/0.0563	18.75	12.7/2.2	7.7	2.5/8.0
7.)	10.61	10.29	0.0987	0.0377/0.061	14.00	14.3/1.7	8.7	1.5/3.7
8.)	10.4	10.1	0.0953	0.0356/0.0597	17.50	15.0/1.5	9.1	3.4/1.6
9.)	8.41	8.16	0.1145	0.0584/0.0561	24.15	4.5/6.5	8.2	5.2/1.6
10.)	8.8	8.6	0.1004	0.0395/0.0609	17.85	14.0/2.0	7.8	1.4/7.0
11.)	5.38	5.22	0.0951	0.0482/0.0469	24.75	4.7/5.2	7.8	1.9/6.0
12.)	8.99	8.73	0.1039	0.0526/0.0513	24.30	4.7/5.2	9.2	2.4/9.0
13.)	4.97	4.82	0.0840	0.0426/0.0414	30.80	4.7/5.2	7.5	1.0/11
14.)	11.7	11.4	0.0948	0.0426/0.0522	7.30	6.7/4.3	8.4	1.3/11
15.)	11.49	11.14	0.1002	0.044/0.0562	20.45	7.7/2.3	7.8	2.8/7.0
16.)	11.9	11.5	0.1083	0.0471/0.0612	14.90	8.0/2.0	7.9	3.0/1.1

The above table contains the instability boundary power and mass flow rates for the sixteen cases done. The period of oscillation was obtained from Fast Fourier Transform (FFT) analyses; this is explained later.

4.3.1 K-factors

Pressure drops were measured by differential pressure transduces across the channel inlet valve, across the heated length and across the channel outlet valve. The measured pressure drops composed of the local pressure drop, frictional pressure drop, and gravitational pressure drop and is represented by equation (4).

$$\Delta P = \Delta P_f + \Delta P_l + \Delta P_g \tag{4}$$

Where

$$\Delta P_f = \sum fr \frac{l}{D} \frac{G^2}{2\rho} \tag{5}$$

$$\Delta P_g = \rho g H \tag{6}$$

$$\Delta P_l = \sum k \frac{G^2}{2\rho} \tag{7}$$

The frictional pressure-drop was calculated by using equation 5, and by applying the same friction factor (fr) formula used by Xiong et al (2012).

The gravitational pressure drop was calculated using the vertical length of the entry and the riser section as represented in equation 6

With the frictional pressure drop and gravitational pressure drop, the k-factors were deduced from equation (4). The k-factor results are summarised in table 4.1 for the sixteen cases.

.

4.4 Non-dimensional parameters

CATHENA code v3.5.4.4 cannot model CO_2 as the working fluid. Hence, it was very important to convert CO_2 data to H_2O accurately. This was done by using the non-dimensional parameters proposed by Ambrosini and Sharabi (2007). These parameters were developed from the classical phase change and sub-cooling numbers adopted in the case of boiling channels. They used pseudo-critical values of density and enthalpy as a function of pressure and formulated non-dimensional parameters. These new non-dimensional parametes reduces the number of variable to be considered in stability analyses to just two variables that are trans-psuedo-critical number and sub-psuedo-critical number.

The parameters are as follows.

$$N_{SPC} = \frac{\beta_{pc}}{Cp_{pc}}\left(h_{pc} - h_{in}\right) \tag{8}$$

$$N_{TPC} = \frac{Q_{in(\exp)}}{m_{in(\exp)}}\frac{\beta_{pc}}{Cp_{pc}} \tag{9}$$

Where: N_{TPC} and N_{SPC} are the trans-pseudo-critical number and sub-pseudo-critical number respectively, β_{pc} represents the isobaric thermal expansion coefficient [K^{-1}], C_p represents the specific heat at constant pressure [kJ kg^{-1} K^{-1}], h represents the specific enthalpy of fluid [kJ kg^{-1}], Q represents the experimental electrical power at boundary [kW], m_{in} represents the experimental mass flow rate at boundary [kg s^{-1}].

To convert the CO_2 data to H_2O, following steps were preformed:

1) Calculate for each inlet temperature and pressure a pseudo-critical point.
2) Get β_{pc} and C_{Ppc} at this point using the NIST property package

3) Using NIST, calculate the inlet enthalpy using the pressure and inlet temperature values used in experiments.

4) Using steps 2 and 3 calculate N_{TPC} and N_{SPC} for all cases.

N_{SPC} and N_{TPC} are calculated for 16 cases and is summarised in table 4:2

Table 4:2: Stability boundary points

Case No.	N_{SPC}	N_{TPC}
1	0.8540	1.2923
2	0.9500	2.7631
3	0.8998	1.8008
4	0.8566	1.3466
5	0.7276	1.7629
6	0.8328	1.5749
7	0.8979	1.7353
8	0.8173	1.6446
9	0.8745	1.2111
10	0.8615	1.4999
11	0.6632	0.9641
12	0.6706	1.2365
13	0.3279	1.0334
14	1.0423	1.9840
15	0.7865	1.9568
16	0.9250	1.8523

5. For water inlet temperature, choose a system pressure (23 MPa say). Use the N_{SPC} values from step 4 and calculate h_{in} and T_{in}.
6. For power, use the N_{TPC} values from step 4, use the same CO_2 velocity, and calculate the mass flow rate and power for water.

The converted stability power and inlet temperature for water for sixteen cases were calculated, and the results are summarised in table 4:3

Table 4:3: Instability boundary data for Water (converted data)

Case	T_{in} [° C]	Power [kW]	Mass Flow [kg/s]	Pressure [MPa]
1	351.6617	56.05	0.0670	23
2	343.6263	71.41	0.0464	23
3	346.3164	90.20	0.0900	23
4	352.2488	59.66	0.0796	23
5	353.109	63.54	0.0648	23
6	354.0521	60.91	0.0695	23
7	348.9137	66.98	0.0694	23
8	355.8817	60.13	0.0657	23
9	364.1809	54.09	0.0802	23
10	351.0894	60.91	0.0730	23
11	363.7194	48.73	0.0685	23
12	365.403	40.32	0.0702	23
13	375.6036	37.81	0.0588	23
14	336.3304	74.74	0.0677	23
15	356.0087	79.00	0.0725	23
16	345.6632	81.29	0.0789	23

4.5 Inlet flow phasing

The inlet flow phasing at the time of instability is discussed in this section. The mass flow rate in both the channels always oscillated 180° out-of-phase as expected. The period of oscillation observed varied from case to case. Two cases with different periods of oscillation are discussed here, namely case 1, and case 5. The period of oscillation in the two cases are 1 second, and 3.2 second, respectively.

4.5.1 Case 1

This case was done at a system pressure of 7.4 MPa and the inlet temperature was maintained at 15.8 °C. The channel inlet valves were fully open, and the channel outlet valves were partially closed (Channel 1 outlet ball valve was 35° closed from the fully open position and Channel 2 outlet ball valve was 40° closed from the fully open position) to impose different outlet k-factors losses. This was done to make the flow asymmetrical in the two channels, which was considered

important in determining the feasibility of flow instability experiments. The asymmetry causes one flow rate to increase while the other decreases to satisfy the mass conservation equation. The channel with low flowrate induces fluctuations and both the channels start to oscillate. (Xiong et al., 2012)

4.5.1.1 Mass flow rate

The system parameters for this case are presented in table 4.1. Instability was observed when the power was increased from 6.6 kW to 6.75 kW. Figure 4.3 shows the mass flow oscillations recorded during the instability. The two-flow rates oscillate out-of-phase, as expected. But an interesting thing to notice is that two type of out-of-phase oscillations exists; one has a short period and the other has a longer period. To better understand this, a Fast Fourier Transform analysis was done on the data, and this is shown in figures 4.4 and 4.5.

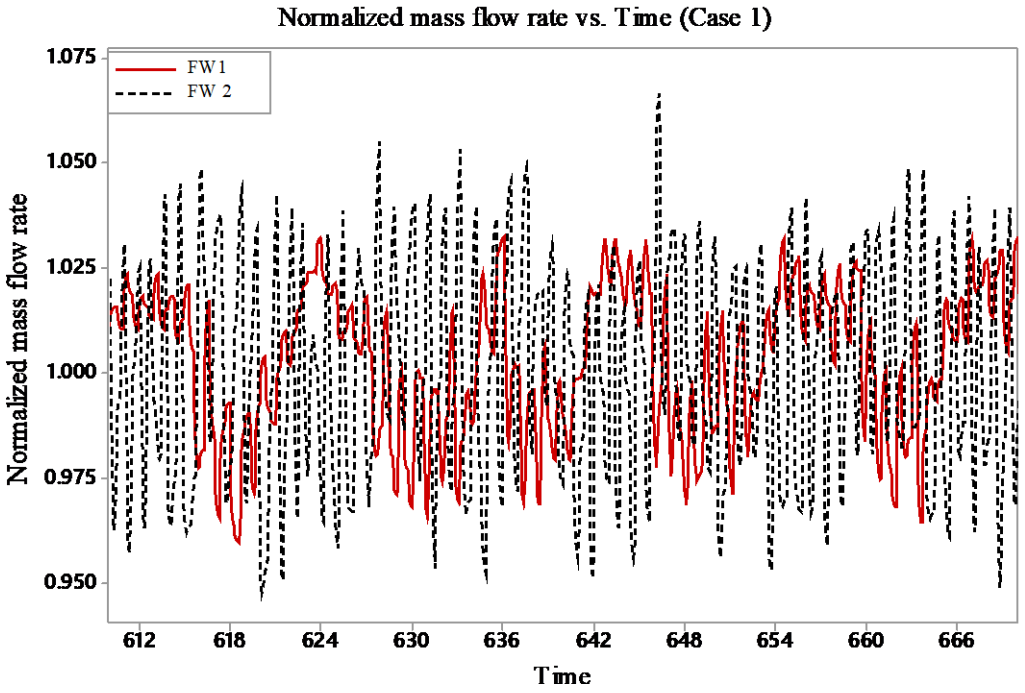

Figure 4.3: Mass flow rate oscillation (Case 1)

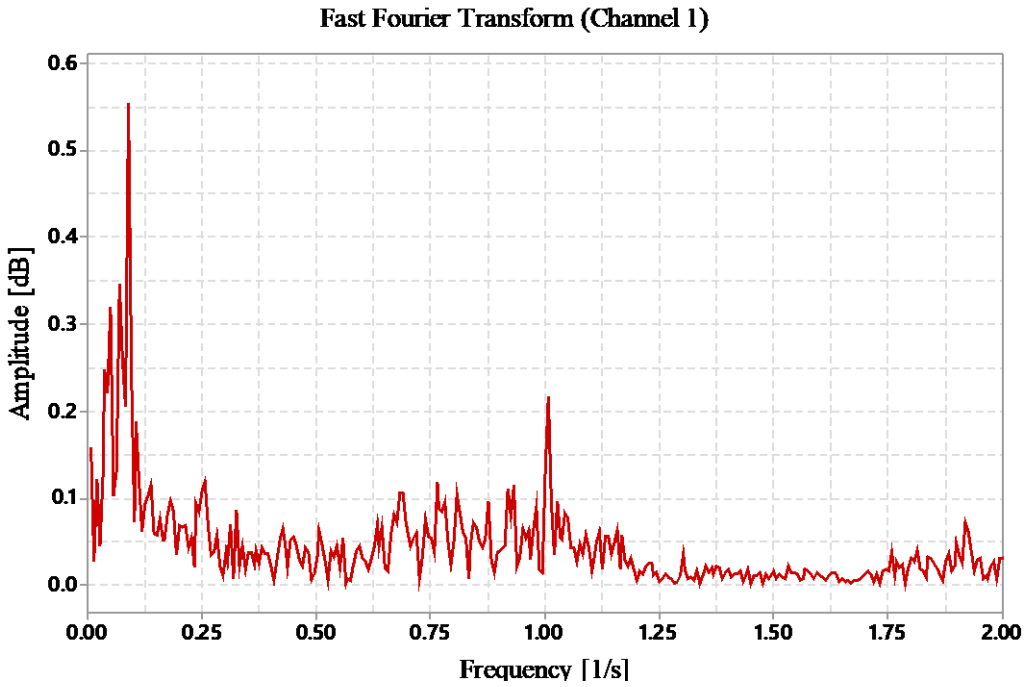

Figure 4.4: FFT Channel 1 (Case 1)

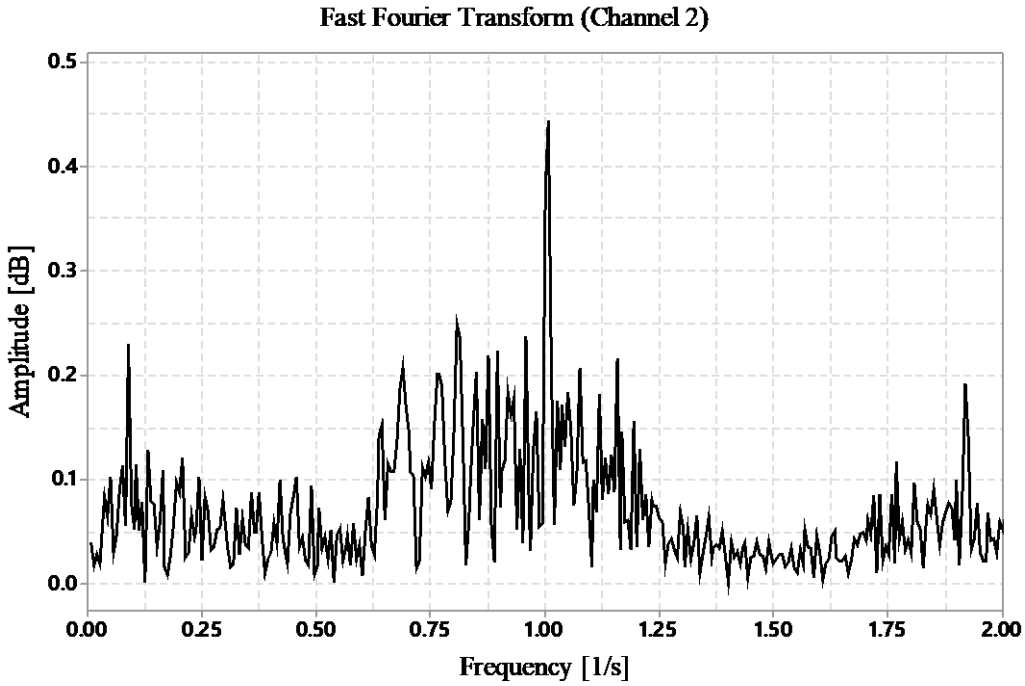

Figure 4.5: FFT Channel 2 (Case 1)

From the above FFT analyses, it can be seen clearly that two different time-period oscillations of 1 second and 11 seconds are present. This dual oscillation period was also uncovered by Ghadge (2018) in Xiong et al. (2012) experimental cases. For Xiong et al. experimental cases, the two periods were ~ 1 and 5 seconds. Previous numerical studies by Li et al. (2016), Xi et al. (2014a) captured the larger period, but not the smaller period. The reason for this was determined by Ghadge et al (2018) to be due to the first order transient scheme. In her analyses, she compared the first order transient scheme and second order transient scheme of CFX and found that the second order transient scheme predicted the smaller period of oscillation, while the first-order transient scheme did not. Moreover, Ghadge (2018) also found that the longer period of oscillation diminished while the shorter oscillation period became more prominent when wall thermal energy storage effects were included in the numerical model. This indicated that modelling wall thermal energy storage effects as well as a higher order time scheme are important for capturing the correct oscillation period. Ghadge (2018) used an in-house linear code (Chatoorgoon and Upadhey (2005)) and found that including the effect of wall thermal energy storage with supercritical Dittus-Boelter correlation not only improved the instability boundary predictions but also predicted the period of oscillation more accurately as compared to no wall thermal energy storage effects.

4.5.2 Case 6

This case was done at a higher system pressure 8.6 MPa and slightly higher inlet temperature, 17.25 °C, than case 1. The channel 1 outlet valve was throttled at 45° from the fully open position, and the channel 2 outlet valve was throttled at 25° from the open position. The onset of oscillation was observed when the electrical power increased from 9.2 kW to 9.4 kW.

4.5.3 Mass flow rate.

Figure 4.6 represents the mass flow rates in two channels during the parallel channel instability. FFT analyses verified that the period of oscillation for this case were 3.2 and 1.6 seconds. Figures 4.7 and 4.8 show the FFT analyses for both the channels.

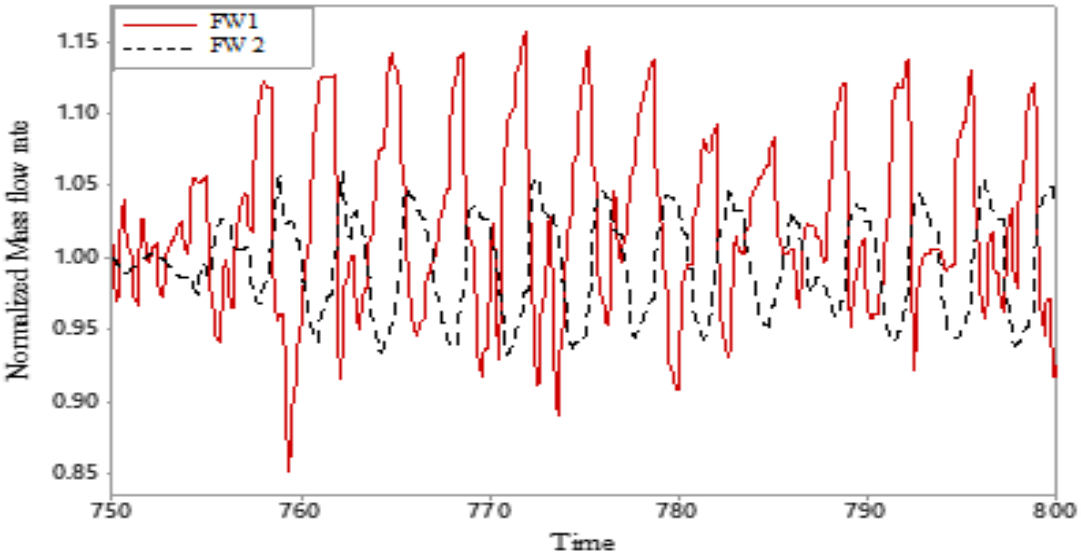

Figure 4.6: Mass flow rate oscillations (Case 6)

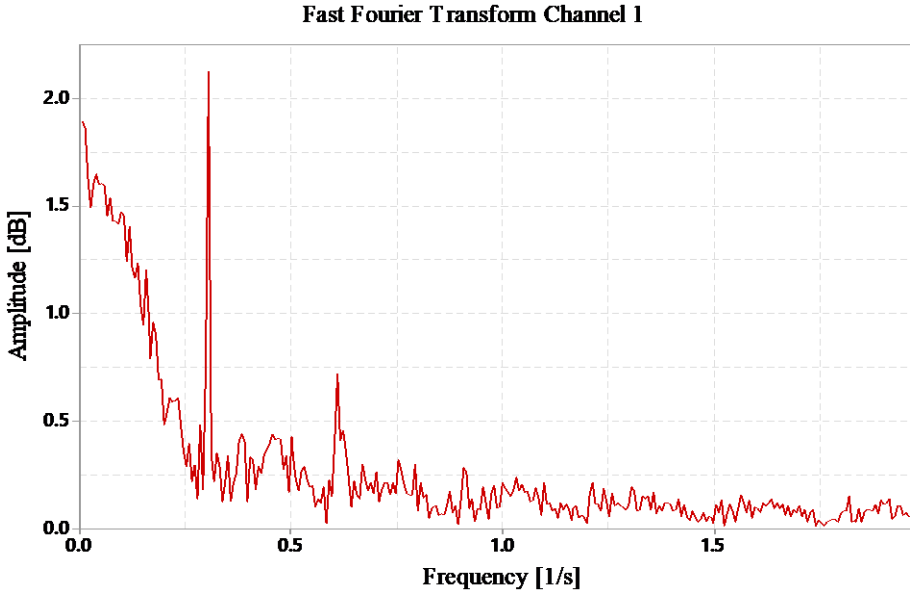

Figure 4.7: FFT Channel1 (Case 6)

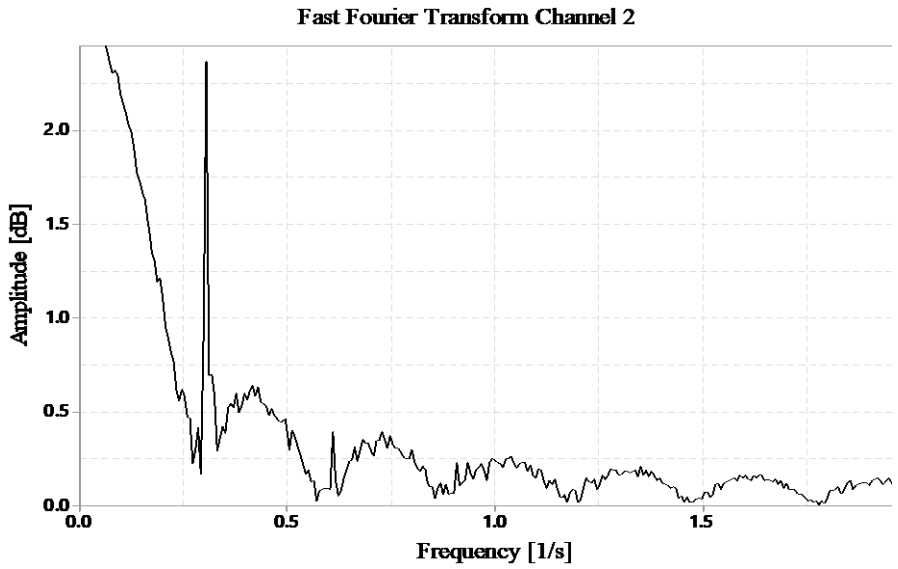

Figure 4.8: FFT Channel 2 (Case 6)

4.6 Summary of Findings.

1) Experiments of flow instability in two vertical heated parallel channels with supercritical CO_2 were carried out to provide useful experimental data with a range of system pressures, inlet temperatures and outlet k-factors. For all the experimental cases, the inlet valves were fully open and only the channel outlet valves were throttled.
2) A total of sixteen instability boundary points was obtained and are presented herein. The major and minor oscillation periods are also presented, obtained from an FFT analysis.
3) While previous experimenters kept their k-factors constant, in this study the channel outlet k-factors were varied from case to case.
4) Two cases are discussed in detail and analogies with previous experiments are drawn.
5) Non-dimensional parameters were used to convert the data into dimensionless form and these+ are tabulated. This data can be used by other modellers to validate their prediction methodology.

Chapter 5 Results: Numerical results and discussion

5.1 Introduction.

In the open literature, two kinds of approaches are used for analysing flow instability: Frequency Domain Method (FDM), and Time Domain Method (TDM). Computer codes using FDM are linear codes that use Linear Stability Analysis in which an infinitesimally small perturbation is added to the linearized governing equations of mass, momentum, and energy; and linear stability theory is used to determine the stability boundary. Non-linear codes work in the real time domain and use finite-difference or finite element or finite volume techniques to approximate the partial derivatives of the 1-D Navier Stokes equation. The resulting algebraic equations are prone to numerical instabilities or a time-step constraint.

In the present study, a licensed 1-D non-linear code, CATHENA, was used to analyse the experimental results of Chapter 4. The version of code used was v.3.5.4.4. This version was used by a previous student to study the stability of a horizontal heater and horizontal cooler natural circulation loop that used supercritical CO_2 as the working fluid (Zhang 2017). An important point to mention here is that the version of the code used cannot model CO_2 directly.

To analyse the current experimental results, a simplified geometry of the SFF-V was used. Non-dimensional parameters proposed by Ambrosini and Sharabi (2007) were used to convert the CO_2 data to corresponding H_2O data in Chapter 4. This numerical study aims to test the capabilities of CATHENA code (v.3.5.4.4) to model supercritical flow instabilities in heated parallel channels with and without thermal energy storage effects.

5.2 Numerical modeling

5.2.1 Introduction to CATHENA (v3.5.4.4) code

The CATHENA code was developed and licensed by Atomic Energy of Canada Limited (AECL). The acronym CATHENA stands for Canadian Algorithm for THErmalhydraulic Network Analysis. This code was developed to analyse the sequence of events that occur during a postulated loss-of-coolant accidents (LOCAs) in Canada Deuterium Uranium reactor (CANDU) or Advanced Candu Reactor (ACR). The code was proved to be useful in simulating a wide range of thermal hydraulic problems in test facilities like CWIT, RD-14 etc. and in small-reactor systems, such as the SLOWPOKE, MAPLE, NRU (Beuthe, 2014).

5.2.1.1 Components in CATHENA

To simulate and model a test facility, components such as pipes, volume, reservoir, tank, T-junction and system models such as discharge model, accumulator model, heat exchanger, junction resistance, pump and valve models are available. Pipe wall modeling can be performed by using the GENHTP, (GENeralized Heat Transfer Package), which allows one-dimensional or two-dimensional conduction of heat transfer in pipes, fuel pins or other conduction materials in contact with the fluid domain.

5.2.1.2 Governing equations

The hydrodynamic model used in CATHENA is a 1-D, two-fluid non-equilibrium model. The model consists of individual mass, momentum and energy equations for the gas and liquid phases together with flow-regime dependent constitutive relations that describe mass, momentum, and energy transfer across the interface and between each phase and the piping walls. The basic hydraulic model consists of six partial differential equation for conservation of mass, momentum

and energy- three for each phase (Hanna, 1998). The governing equations are documented in Beuthe, (2013)

5.2.1.3 Solution of the governing equations

To solve these equations, staggered mesh, one-step implicit first-order, donor-cell upwind differencing scheme over control volumes or nodes are adopted. Moreover, as the supercritical fluid is a single-phase fluid and can exist either as liquid or vapour, a constant void fraction of 0.0 is set automatically. The conservation equation for only one state are used. When GENHTP model is used with supercritical conditions, the heat transfer correlation is automatically set to Dittus-Boelter correlation (developed for heat transfer from subcooled single-phase liquid in tubes).

$$h_f = 0.023 \frac{K_f}{D_e} \mathrm{Re}_f^{0.8} \mathrm{Pr}_f^{0.4} \qquad (10)$$

where h_f is the heat transfer coefficient [W-m^{-2}-K^{-1}], K_f is the fluid thermal conductivity [W-m^{-1}-K^{-1}], Re_f is the fluid Reynolds number, Pr_f is the fluid Prandtl number.

More details on the numerical method used to solve the governing equations are omitted here and can be found in Beuthe (2013)

5.2.1.4 Property package

CATHENA uses Piecewise Hermite Polynomial Approximation to generate functions for thermophysical properties of both light water (H_2O) and heavy water (D_2O) for subcritical pressures. To extend the code capabilities to model supercritical pressures, an alternative set of light water property fits based on the IAPWS was added. This addition extends the light water properties from P_{min} = 611.657 Pa to P_{max} = 100 MPa and the critical point of H_2O occurs at pressure, P_{cr} = 22.0703 MPa and temperature, T_{cr} = 373.936 °C. A user-controlled parameter called 'Numeric Option' is required to enable the code to use the additional water properties. The variable

'HLWP-VERSION (1)' allows the code to model thermal hydraulic networks at supercritical pressure conditions.

5.2.2 Benchmarking of CATHENA.

The code has only been benchmarked against experiments for heat transfer to supercritical water flowing in vertical tubes (Hanna, 2010). The findings showed that CATHENA yielded reasonable agreement with those experiments. However, the inside surface wall temperature profile results diverged as the fluid temperature in the pipe passed through the pseudo-critical enthalpy region. The CATHENA code (v.3.5.4.4) was also used to determine the stability boundary of the SFF-H (Zhang, 2017). Zhang's study concluded that the CATHENA code v 3.5.4.4 can capture flow instability in a natural circulation loop under supercritical conditions with H_2O. However, that study was performed without consideration of wall thermal energy storage effects. Before simulating the current experimental data, it is of utmost importance to check if the current version of the CATHENA code can predict flow instability boundary well for two vertical parallel channels with supercritical water.

5.2.3 Physical model.

To simulate these experiments with CATHENA, a simplified model of SFF-V was used, which is represented in fig 5.1. The simplified model consisted of two reservoir boundary conditions at inlet and outlet, namely 'LOWBC' and 'UPBC' to simulate constant pressure conditions inside the loop (refer figure 5.2). The Junction resistance model was used to represent the four valves on the geometry. The experimental mass flow rate was used in the simulations as the inlet mass flow condition.

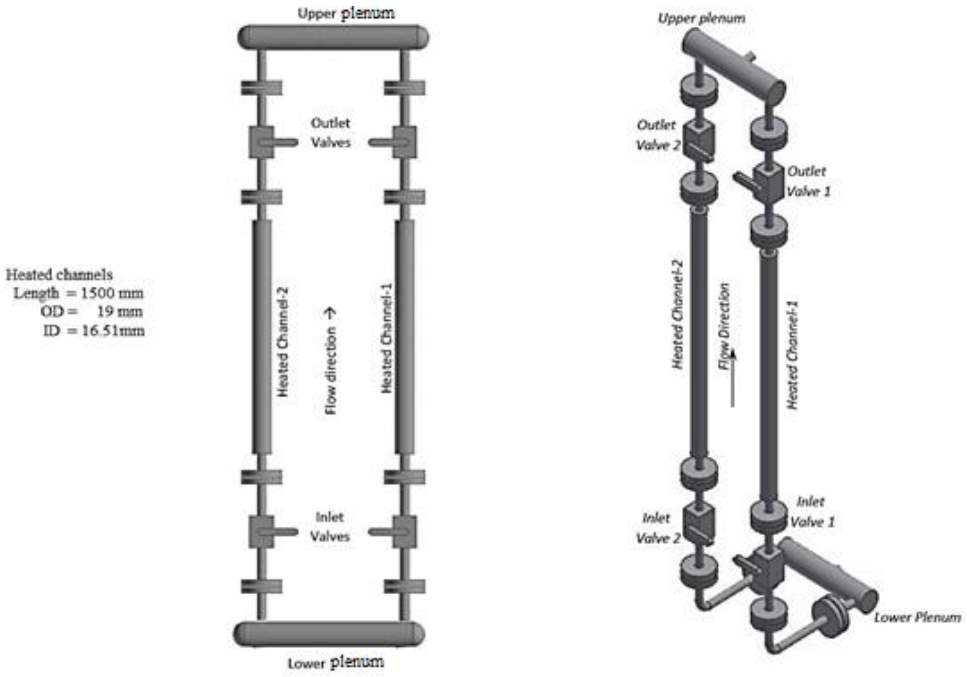

Figure 5.1: Simplified geometry of SFF-V for modeling in CATHENA code.

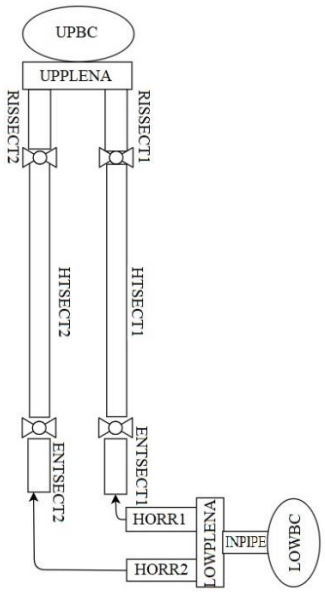

Figure 5.2: Nomenclature of components used in CATHENA code.

5.3 Assumptions

The following assumptions were made with regard to modelling the experiments:

a) The heat is uniformly applied to the fluid and heat loss is ignored.

b) Heat conduction in axial direction is neglected.

c) Four junction resistances are considered for the four ball valves.

d) The diameter is taken as constant for all the pipe components as the local pressure drop is included in the calculation of the k-factors.

e) No wall model is considered for reasons explained in section 5.8.2

5.4 Boundary Conditions.

- Specified total mass flow rate at inlet
- Specified inlet temperature at inlet
- Specified loop pressure.

5.5 CATHENA (V.3.5.4.4) code results

Firstly, the CATHENA code was used to model the instability experiments of Xiong et al., 2012 and Xi et al., 2014b. The aim was to directly test the capability of CATHENA code (v. 3.5.4.4) to predict instability boundary with and without wall thermal energy storage effects. The experimental facility of Xiong et al. consisted of two vertical parallel channels with 6 mm and 11 mm inner and outer diameters, respectively. The experimental facility also consisted of a lower plenum, flow meters, entrance sections, riser sections and an upper plenum. Figure 5.3 gives a schematic of the test section and figure 5.4 gives the simplified geometry proposed by Xiong et al. to be used for modelling. The test section was made of INCONEL 625 alloy pipes with a length of 3000 mm. Moreover, the whole loop piping was insulated to minimize heat losses to the

environment. Sheathed N-type thermocouples measured fluid temperature at inlet and outlet of the test section. Wall temperatures were measured with 14 N-type thermocouples spaced along each heated pipe at seven different axial locations. Two venturi flow meters calibrated with H_2O at supercritical pressures were used to accurately measure the mass flow rates of the two channels. Pressure measurements were made at the lower plenum, inlet of the heated section, outlet of the heated section and upper plenum. Heat was supplied to the test section via a DC power supply and was measured through current and voltage readings. More details can be found in Xiong et al. (2012)

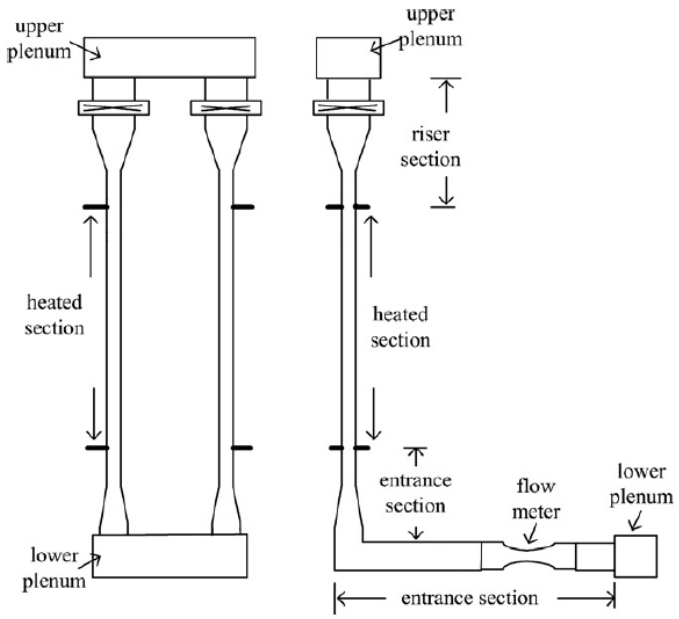

Figure 5.3: Schematic of test section

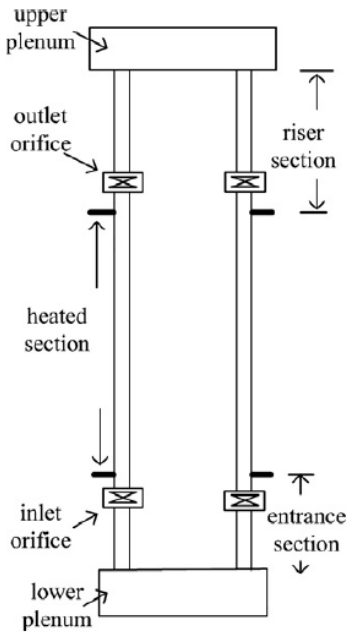

Figure 5.4: Proposed loop for modeling

Xi et al. (2014) used the same experimental facility to perform more experiments and to continue the flow instability study with thicker walls. The aim for using thicker walls was to suppress the instability and make the system more stable. A wall thickness of 6.5 mm was used. The length of the test sections was 3105 mm. In addition to this, three copper plates place at equal distance was used to divide the test section into two parts axially. This was done to study the influence of different axial power shape. The rest of the loop components remained the same. However, water-cooled insulation flanges at the inlet and outlet of each pipe was used for better sealing and insulation. The power supply was controlled independently for the two parts of the heated channels using a group of modular DC power supply. The geometry for modeling in CATHENA was like the one used for the previous experimental study (Xiong et al., 2012) except for the length of the heated channels, which was 3105 mm instead of 3000 mm.

The geometry shown in fig 5.4 was modelled by using nine pipe components. The dimensions of the lower and upper plenum were not reported in both experimental studies. So, dimensions based on a CFX study done by Ghadge (2018) was used for modeling in CATHENA. Figure 5.5 shows the detailed dimensions used. Before doing any numerical study, it is important to see if the results are sensitive to grid refinement and time step.

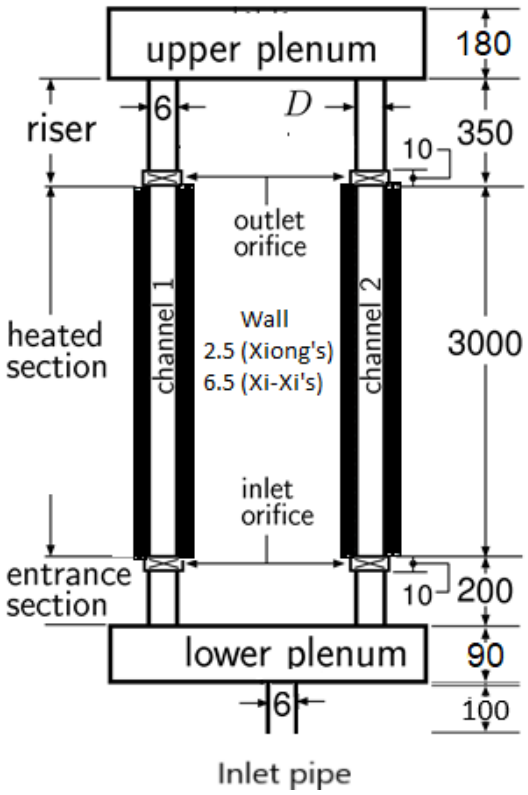

Figure 5.5: Dimensions (in mm) and geometry used for simulation in CATHENA.

5.6 Sensitivity test of numerical discretization parameters.

As the literature suggests (Ebrahimnia et al., 2016; Li et al., 2018; Shitsi et al., 2017) the flow instability boundary prediction can be significantly affected by grid size or time step. So, it is of vast importance to first find the optimum grid size and time step. The flowing subsections present

a study performed to determine the optimum grid size and time step for spatial and temporal independent results.

5.6.1 Effect of Spatial grid refinement

To ensure that the numerical result was independent of grid refinement different number of nodes 50,200,400,600 were used on the heated section. To check for convergence, a base case was selected from Xiong et al. ‘s experimental data (Case 9), and the steady state solution was obtained for different number of nodes. The steady state solution was then analysed to get fluid temperatures at outlet of the channels. It was observed that increasing the number of nodes from 50 to 200 there was a sharp change in the outlet temperature and then as the number of nodes was increased further the outlet fluid temperature converges. Fig 5.6 shows the fluid temperature at the last node near the exit of the channel vs the number of nodes. Four hundred nodes were selected for the heated channels to get grid independent converged results.

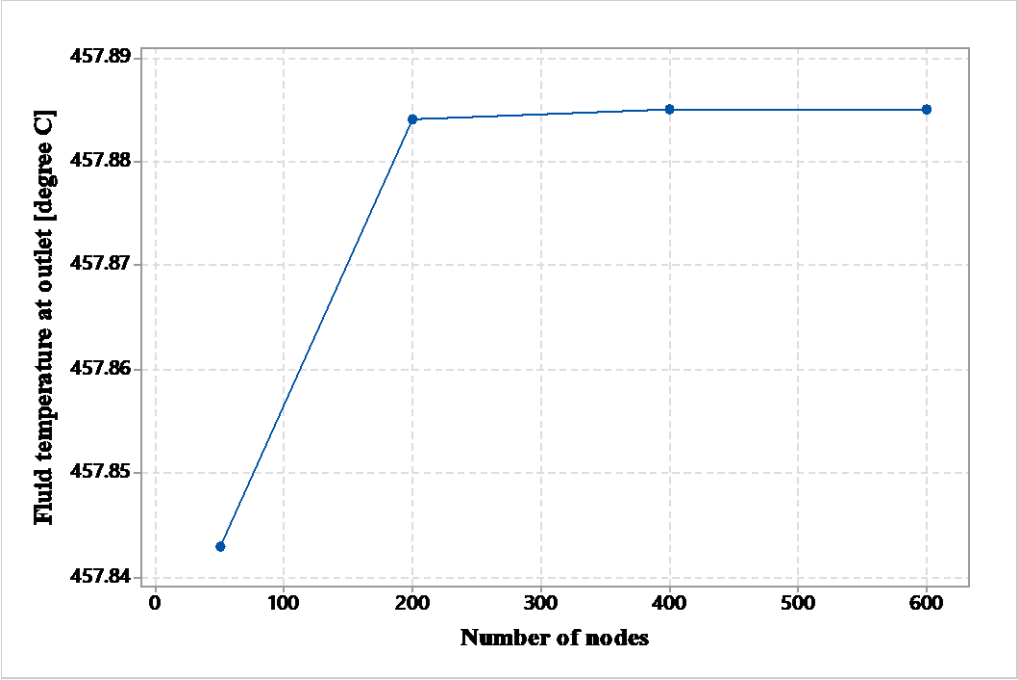

Figure 5.6: Steady state outlet fluid temperature with different number of nodes (Case 9)

Additionally, the effect of grid refinement on prediction of stability boundary was also studied. Three configurations of node numbers were used: 50, 400, and 600. The transient response of the three configurations were obtained, and it was found that the difference in prediction with 50 nodes on the heated channels and 400 nodes was not significant. The number of nodes was increased from 400 to 600, that difference became zero. Table 5:1 summarises the stability boundary power of the three configurations.

Table 5:1: Effect of number of nodes on Stability boundary power

Number of nodes (#)	Stability boundary power [kW]	Difference %
50	63.4	0.63 %
400	63.0	0.00 %
600	63.0	-

5.6.2 Effect of Temporal grid refinement.

To study the effect of temporal grid refinement, a base case of Xiong et al. experimental data (Case 9) was selected. The system pressure of 25 MPa, inlet temperature of 239.85 °C and a power of 31.5 kW per channel which is lower than the instability threshold was selected and time steps of 0.1, 0.01, and 0.001 seconds were used to show its effects on the flow oscillations and instability boundary power. In all the cases, the number of nodes used on the heated channels were 400 (explained in section 5.6.1). Figure 5.7 shows the flow oscillations for the three different time steps; as the time step was reduced the flow oscillation pattern converges. Moreover, the instability boundary power predicted by three-time steps vary. Table 5:2 shows the effect of time step refinement on instability boundary power. The difference between the stability predicted by time step of 0.001 s and 0.01 s was about 0.8%, whereas with a time step of 0.1 s the difference was

3.19%. A time step of 0.01 s was thereby chosen as the acceptable compromise of accuracy and computational effort.

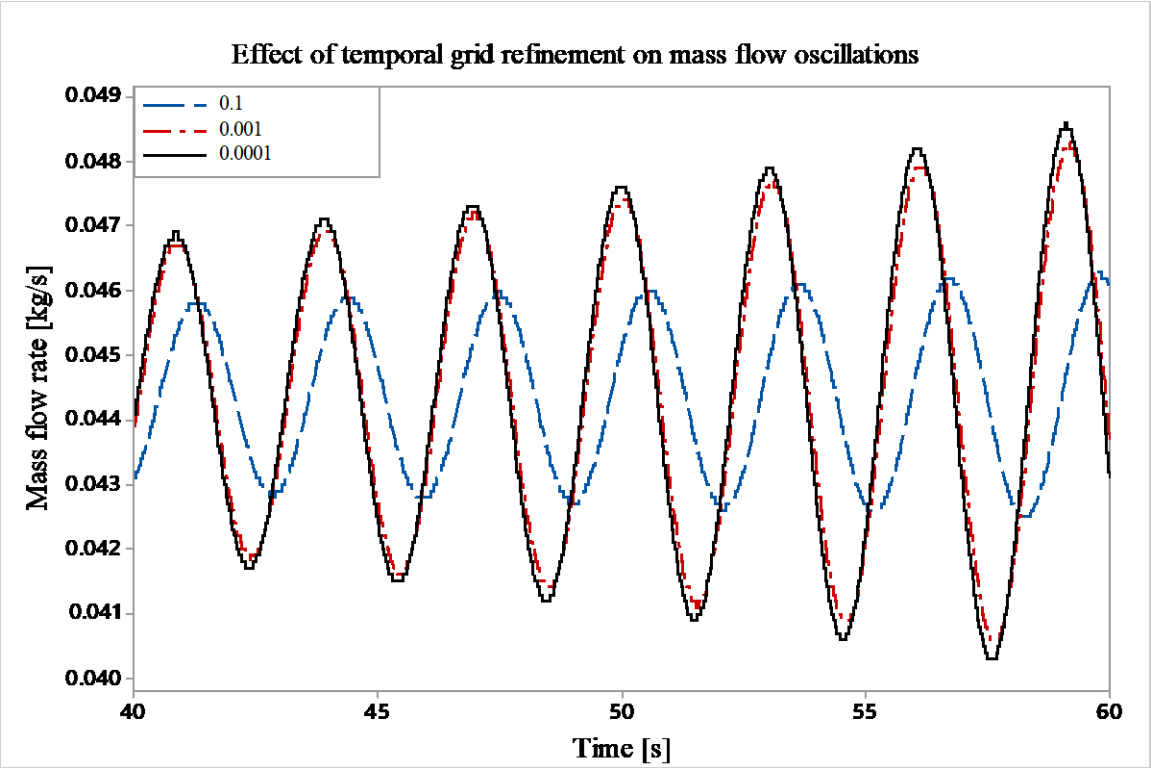

Figure 5.7: Mass flow oscillation pattern for different time steps (Case 9)

Table 5:2: Effect of time step size on stability boundary

Stability boundary power [kW]	Time step [s]	Difference %
64.6	0.100	3.19%
63.0	0.010	0.8%
62.6	0.001	0.0%

Similar kind of studies were carried out for Xi et al. (2014) experiments and the present CO_2 experiments to ensure the numerical predictions were independent of Spatial grid and temporal grid refinement. Table 5:3 shows the number of nodes in the heated section and time steps used for the three numerical studies.

Table 5:3: Parameters chosen for three different studies

Experiments	Number of nodes (#)	Time step (s)
Xiong et al 2012	400	0.01
Xi et al 2014	600	0.01
Present	900	0.001

5.7 Experimental Results of Xiong et al and Xi et al.

5.7.1 Xiong et al (2012) Experimental results.

The experiments performed by Xiong et al. (2012) used different flow conditions with a pressure range of 23 MPa to 25 MPa, inlet temperature ranging from 453 K to 513 K. The instability boundary results with different conditions are summarized in table 5:4.

Table 5:4: Experimental results table Xiong et al (2012)

Cases	System pressure (MPa)	Inlet temperature (K)	Total inlet mass flow rate (kg/s)	Total power (kW)
1	23	453	0.0342	67.9
2	23	473	0.0333	66.0
3	23	493	0.0333	65.6
4	24	473	0.0333	67.0
5	24	493	0.0333	66.0
6	24	513	0.0331	64.6

7	25	473	0.0328	69.3
8	25	493	0.0333	68.9
9	25	513	0.0339	67.9

The instability boundary powers were obtained by fixing the total mass flow rate at the inlet and varying the heating power until the channel inlet mass flow rate started oscillating out-of-phase.

5.7.2 Xi et al. (2014) cases

Xi et al. (2014) performed experiments with different axial power shape, but in the present study, only the five cases with uniform power distribution were modeled. The five cases had a system pressure of 23 MPa with inlet temperature ranging from 453 K to 533 K at a constant mass flow rate of 125 kg/h (0.0347 kg/s). Similar approach to Xiong et al. (2012) was used to find the instability boundary. Table 5:5 summarises the five uniform power cases.

Table 5:5: Experimental results table Xi et al (2014)

Cases	System pressure (MPa)	Inlet temperature (K)	Total inlet mass flow rate (kg/s)	Total power (kW)
1	23	458	0.0347	79.02
2	23	479	0.0347	77.22
3	23	495	0.0347	76.21
4	23	513	0.0347	72.91
5	23	533	0.0347	71.42

5.8 Comparison of CATHENA predictions with experimental results of Xiong et al and Xi et al

5.8.1 Without wall thermal energy storage effect.

5.8.1.1 Xiong et al. (2012) Cases

The comparison of experimental threshold power and CATHENA code predictions are shown in table 5:6. It was found that CATHENA code could predict most of the cases with good agreements. However, it was also found that for cases 1(P = 23 MPa, T_{in}= 453 K), 2(P = 23 MPa, T_{in}= 473 K), and 4(P = 24 MPa, T_{in}= 473 K) the steady state did not converge. The code took longer simulation time to converge the initial steady state mass flow rate when the power was near the experimental instability power. No instability was observed when a transient was initialized from the previous steady state results. If the power was increased further, the mass flowrate in steady state simulation oscillated and did not converge no matter how long the simulation ran. The oscillation of mass flow rate was numerical. Figure 5.8 shows the steady state simulation result for Case 2, the total heating power used in the simulation is 65.8 kW (32.9 kW per channel), the simulation ran for 15000 s. The steady state solution does not converge. Similar type of behaviour was observed in the other two cases. The reason for this may be the property packages used in CATHENA.

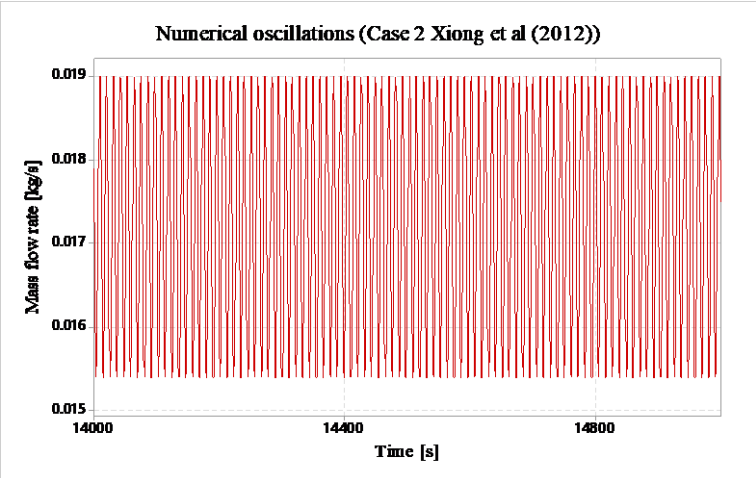

Figure 5.8: Steady state solution (simulated for 15000 s), Mass flow rate oscillations (Case 2)

Table 5:6: Comparison of numerical predictions (without wall) with experimental results Xiong et al. (2012)

Case	Experimental	Numerical code predictions			
		CATHENA (Present Study)		Linear (Ghadge et al 2018)	
	Power (kW)	Power	Difference	Power	Difference
1	67.9	*	-	65.5	3.53
2	66.0	*	-	63.5	3.79
3	65.6	62	5.49	62.5	4.73
4	67.0	*	-	63.5	5.22
5	66.0	63.5	3.78	64	3.03
6	64.6	60	7.12	62	4.02
7	69.3	65.4	5.63	67	3.32
8	68.9	64.5	6.39	68.1	1.16
9	67.9	63.0	7.23	66	2.80

* steady state mass flow rate did not converge for these 3 cases.

5.8.1.2 Xi et al. (2014b) Cases

Five cases of Xi et al. uniform power profile cases were simulated with CATHENA. The comparison of the code predictions and experimental results are summarised in table 5:7. A maximum error of 15.29% was found between code predictions and experimental results. Also, case 1 has similar numerical oscillations reported in section 5.8.1.1. The inlet temperature for this case was 458 K and the pressure was 23 MPa.

Table 5:7: Comparison of numerical predictions (without wall) with experimental results Xi et al. (2014b)

Case	Experimental	Numerical code predictions			
		CATHENA (Present Study)		Linear (Ghadge et al 2018)	
	Power (kW)	Power	Difference	Power	Difference
1	79.02	*	-	78	-1.29
2	77.22	67.6	12.45	76.2	-1.33
3	76.21	65.6	13.92	74.5	-2.25
4	72.91	63.0	13.59	71.2	-2.34
5	71.42	60.5	15.29	69.8	-2.27

* steady state mass flow rate did not converge.

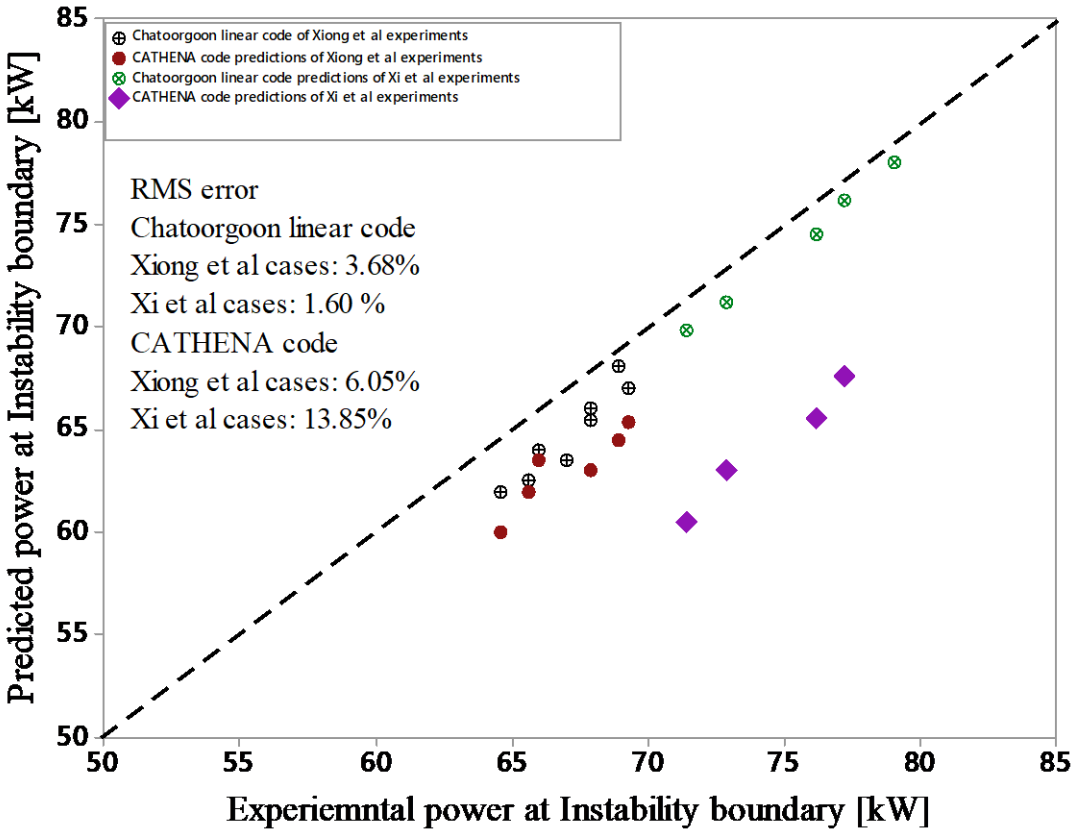

Figure 5.9: Comparison of Numerical code predictions (without wall) with Experimental results

5.8.2 With wall thermal energy storage effect.

The radial conduction wall models in CATHENA were included in simulating four experimental cases: Case 3, Case 5, Case 7 and Case 9 of Xiong et al. (2012). Axial condition was neglected in this simulation due to recommendations made in a previous study by Ghadge et al. (2018). As in the experiment, a wall thickness of 2.5 mm was used with five nodes in the radial direction. In the axial directions, there is maximum limit of 50 nodes that can be used (using more than 50 nodes gives an error and the simulation ends) so to increase the node in axial direction to 300, the axial length of 3000 was divided into six sections with 50 nodes. The power was uniformly applied over the whole wall model.

No unstable behaviour was observed even when the power per channel exceeded 50 kW per channel. A study was done to check the sensitivity of the instability boundary power predictions to wall thickness.

5.8.2.1 Instability boundary power sensitivity to wall thickness

Mathematically, when the thickness of the channel tends to zero, the results predicted should be close to the no wall results. Hence, Case 9 was selected from the experimental data obtained by Xiong et al. (2012) for which a power of 63 kW was predicted without the wall thermal energy storage effect by CATHENA code (refer table 5.6). Three different wall thicknesses 0.01 mm, 0.1 mm and 0.5 mm were used to check for sensitivity. The instability power of the three cases predicted by the code are summarized in table 5:8.

Table 5:8: Wall thermal heat storage effect study (Case 9)

No wall instability boundary power [kW]	Wall thickness [mm]	With wall instability boundary power [kW]
63.0	0.01	64.9
63.0	0.1	87.9

63.0	0.5	114.9

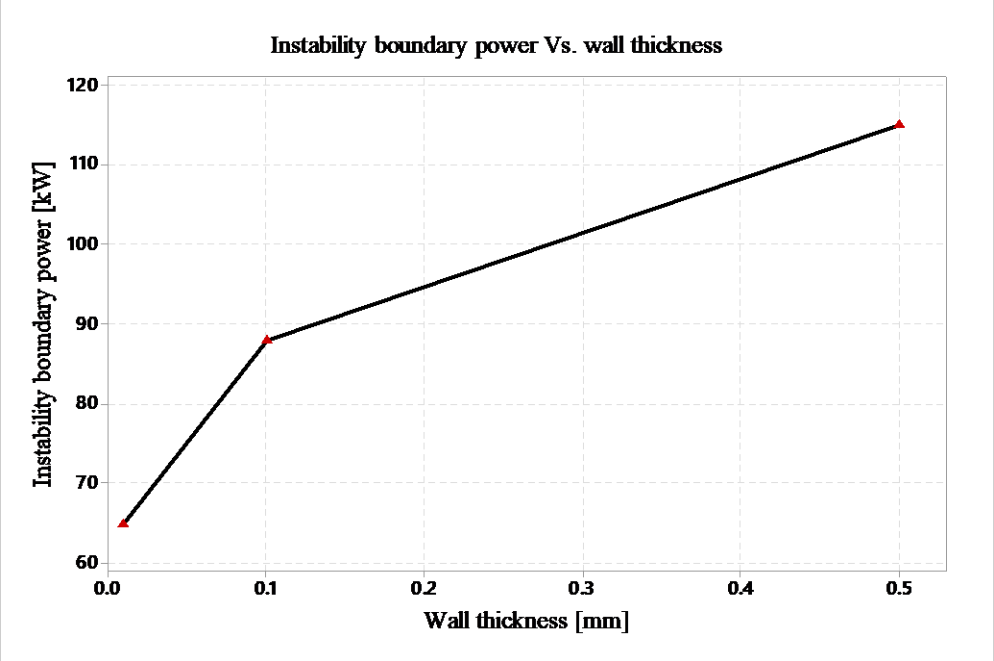

Figure 5.10: Instability boundary power predictions with different wall thicknesses (Case 9)

From the table and plot (figure 5.10), with a thickness of 0.01 mm, CATHENA predictions are approaching the no wall predictions. However, with an increase of 0.09 mm in wall thickness, the code predictions become unrealistically large. A maximum error of 29.45% was obtained in the numerical predictions. The finding here was that the wall model in CATHENA are unable to predict realistic stability boundaries and, hence, no further studies were done with wall effects.

5.9 Comparison of CATHENA code predictions with present experimental results

5.9.1 Steady state mass flow rate.

As the steady state mass flow rate plays a significant role in determining the transient response, the correct prediction of the mass flow rate is of utmost importance. Table 5:9 summarises the calculated total mass flow rate for H_2O data using the non-dimensional parameters and the predicted mass flow rate split between the two channels using CATHENA code v.3.5.4.4.

Table 5:9: Mass flow rate splits predicted by CATHENA code vs present study experiments

Case number	Calculated total Mass flow rate [kg/s]	Predicted mass flow rate [kg/s]	
		Ch1	Ch2
1.)	0.0670	0.0337	0.0333
2.)	0.0464	0.0237	0.0227
3.)	0.0900	0.0465	0.0435
4.)	0.0796	0.0396	0.0373
5.)	0.0648	0.0295	0.0353
6.)	0.0695	0.0326	0.0369
7.)	0.0694	0.0312	0.0382
8.)	0.0657	0.0303	0.0354
9.)	0.0802	0.0407	0.0395
10.)	0.0730	0.0335	0.0395
11.)	0.0685	0.0344	0.0341
12.)	0.0702	0.0372	0.0330
13.)	0.0588	*	*
14.)	0.0677	0.0305	0.0372
15.)	0.0725	0.0302	0.0423
16.)	0.0789	0.0333	0.0456

* Steady state mass flow did not converge.

5.10 CATHENA Stability predictions.

Table 5:10 shows the comparison of experimental results with CATHENA stability predications. Sixteen cases were simulated out of which 13 cases yielded reasonable agreement with the

experiments with an RMS error of 10.39%. Case 13 had an inlet temperature close to the pseudo-critical point, which may be the reason for the steady state simulation to not converge.

Table 5:10: Comparison of stability boundary power experimental vs numerical

Case number	Experimental results	CATHENA code predictions	
	Power [kW]	Power [kW]	Difference %
1	56.0	60.0	-7.14
2	71.41	61.0	14.57
3	90.20	80.0	11.30
4	59.66	49.8	16.52
5	63.54	59.0	7.14
6	60.91	57.6	5.43
7	66.98	64.0	4.45
8	60.13	49.0	18.30
9	54.09	52.0	3.86
10	60.91	50.0	17.91
11	48.73	41.0	15.86
12	40.32	36.3	9.97
13	37.81	*	
14	74.74	71.0	5.0
15	79.00	76.8	2.78
16	81.29	79.4	2.32

* Steady state mass flow did not converge.

The above CATHENA results were obtained by fixing the total mass flow rate at inlet and specifying constant pressure boundary and varying the power. Additionally, figure 5.11 shows a comparison between experimental stability power with CATHENA predictions in a plot

5.10.1 Period of oscillation.

It is of vast importance to predict the correct period of oscillation along with the instability boundary power and mass flow rate. In this study, the CATHENA code always predicted the same period of 3.33 seconds for every case in the three experimental studies, whereas the period of oscillation varied from cases to case in the experiments. The accurate prediction of period of oscillation was first reported by (Ghadge, 2018) for Xiong et al and Xi et al experiments. Ghadge

et al found that the period of oscillation depends on the transient scheme used. The second order transient scheme provide more accurate results than the first order transient scheme. She also used an in-house linear code (Chatoorgoon V., and Upadhye P. 2005) and concluded that the linear, frequency-domain solution predicts accurately the period of oscillation.

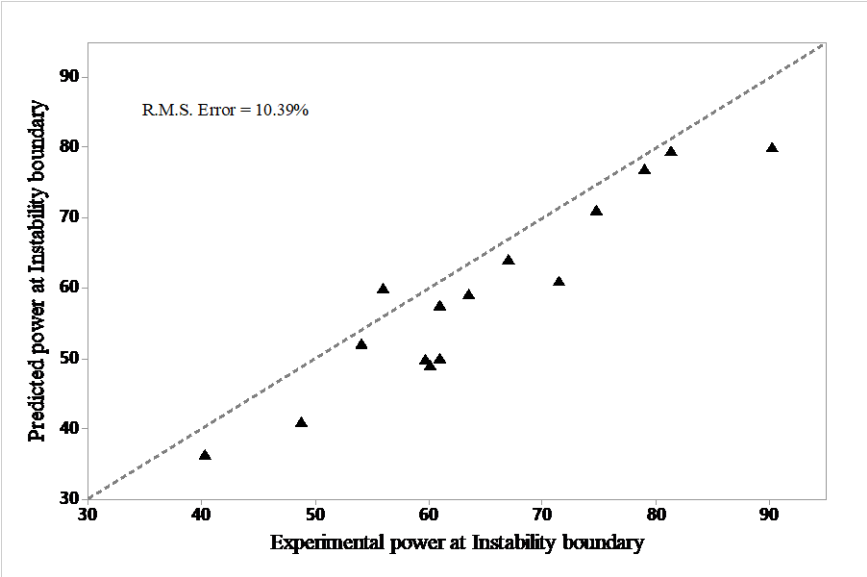

Figure 5.11: Comparison of Saini's Experimental instability power with CATHENA code predictions

5.11 Summary of Findings

The CATHENA code (v. 3.5.4.4) was used for the first time to model two parallel heated channels with CO_2 data converted to H_2O. The results obtained are summarised below:

1) The numerical predictions of instability boundary power for previous experimental studies agreed well for some cases but the period of oscillation was inaccurate. Also the CATHENA results are quite inaccurate when compared to the linear code results reported by Ghadge et al (2018). It was found that, for cases with an inlet temperature $\leq$ 475 K and system pressure $\leq$ 24 MPa, the steady state simulation results did not converge. The reason for this may be the property package in the CATHENA code.

2) The inclusion of wall thermal heat storage effects showed that the CATHENA code (v.3.5.4.4) gives unrealistic results.
3) The numerical predictions (without wall) of current experiments agree with an RMS error of 10.39%. However, for some results have a maximum error of 18.30%.

Chapter 6 Summary, conclusion, and future recommendations.

In this chapter, the summary of the present research is provided. In addition to this, meaningful conclusions are drawn from the results, and future recommendation are also listed.

6.1 Summary.

The present research deals with the supercritical flow instabilities in two vertical parallel heated channels using CO_2. The main objectives of the study were to capture parallel channel instability data under different working conditions, to access the ability of CATHNEA code v.3.5.4.4 to model the supercritical flow instabilities with and without the wall thermal energy storage effect.

The above objectives were realised by conducting experiments on the Supercritical flow facility-vertical, which is constructed at the University of Manitoba. Moreover, the CATHENA code v3.5.4.4 was used to model two previous experimental studies of Xiong et al (2012), Xi et al (2014b) and present experiments to asses its ability in modeling the supercritical flow instabilities. The flowing subsections provides the conclusions of this study.

6.2 Conclusions

Both experimental and numerical studies were performed in the present work. Below are relevant conclusions drawn form the results obtained.

6.2.1 Experimental results.

1) Experiments of flow instability in two vertical heated parallel channels with supercritical CO_2 were carried out at University of Manitoba to provide experimental data with a wide range of system pressures, inlet temperatures and outlet k-factors. For all the experimental cases, the inlet valves were fully open and only outlet valves were throttled.

2) A total of sixteen instability boundary points was obtained and are presented herein. The oscillation periods are also presented, obtained from an FFT analysis.
3) While previous experimenters kept their k-factors constant, in this study the channel outlet k-factors were varied from case to case.
4) Two cases are discussed in detail and analogies with previous experiments are drawn.
5) Non-dimensional parameters were used to convert the data into dimensionless form and they are tabulated. This data can be used by other modellers to validate their prediction methodology.

6.2.2 Numerical results

1) The numerical instability boundary predicted by CATHENA code v 3.5.4.4 for previous experimental cases (Xiong et al., 2012; Xi et al., 2014b) provided a reasonable agreement with exception of some cases [refer section:5.8.1]. But, the period of oscillation predicted by the code is not accurate. Moreover, the results predicted by the CATHENA code are quite inaccurate when compared to linear code results reported by Ghadge et al (2018)
2) The effect of grid refinement on the prediction of instability boundary had negligible effect.
3) CATHENA code instability boundary predictions were sensitive to time step size. Large time step overpredicted the power by 3.19 %.
4) Using the wall model in CATHENA code predicted unrealistic results for the instability boundary.
5) The numerical prediction of instability boundary power in the present study agrees with an RMS error of 8.32%. However, for two cases (Case 9 and Case 11) the power is overpredicted by a maximum of 25%.

6) The period of oscillation predicted by CATHENA code for the three experimental studies is 3.33 seconds, which is obviously not correct. The reason for this is suspected to be the first order transient scheme used in CATHENA code v3.5.4.4

6.3 Future recommendations

1) The turbine flow meters used for present study were calibrated for the upper 70% range using water. However, the flow rate obtained in the present study was in the lower 30% range, which underestimates the flow rate by ± 2%. A new flow meter with a smaller measurement scale could be used instead of the current one.
2) More experimental cases with lower inlet temperature should be done to get more insight to the supercritical flow instability.
3) A supercritical flow pump should be used to study vertical down flow.
4) A new system for pressure regulation should be installed as the current one involves the operator to leave the monitor to release excess pressure form valves.
5) Newer version of CATHENA code should be used to model the current facility with CO_2 as the working fluid for further comparison with the experimental data.
6) The wall models in CATHENA should be improved, as the results predicted by the current version (v.3.5.4.4) are unrealistic.
7) Higher order transient scheme should be included in newer version of CATHENA code to accurately predict the period of oscillation.

References

Ambrosini, W. (2007). On the analogies in the dynamic behaviour of heated channels with boiling and supercritical fluids. Nucl. Eng. Des. *237*, 1164–1174.

Ambrosini, W., and Sharabi, M. (2007). Dimensionless parameters in stability analysis of heated channels with fluids at supercritical pressures. Nucl. Eng. Des. *238*, 1917–1929.

Ampomah-Amoako, E., and Ambrosini, W. (2013). Developing a CFD methodology for the analysis of flow stability in heated channels with fluids at supercritical pressures. Ann. Nucl. Energy *54*, 251–262.

Ampomah-Amoako, E., Akaho, E.H.K., Nyarko, B.J.B., and Ambrosini, W. (2013a). Analysis of flow stability in nuclear reactor subchannels with water at supercritical pressures. Ann. Nucl. Energy *60*, 396–405.

Ampomah-Amoako, E., Akaho, E.H.K., Nyarko, B.J.B., and Ambrosini, W. (2013b). CFD analysis of the dynamic behaviour of a fuel rod subchannel in a supercritical water reactor with point kinetics. Ann. Nucl. Energy *59*, 211–223.

Beuthe, T. (2013). Cathena Theory manual.

Beuthe, T.G. (2014). CATHENA code Abstract v. 3.5.4.4.

Boure, J.A., Bergles, A.E., and Tong, L.S. (1973). Review of two-phase flow instability. Nucl. Eng. Des. *25*, 165–192.

Chatoorgoon, V. (1986). SPORTS - A simple non-linear thermalhydraulic stability code. Nucl. Eng. Des. *93*, 51–67.

Chatoorgoon, V. (2007). Supercritical flow stability in horizontal channels. Nucl. Eng. Des. *238*, 1940–1946.

Chatoorgoon, V. (2013). Non-dimensional parameters for static instability in supercritical heated channels. Int. J. Heat Mass Transf. *64*, 145–154.

Chow, C.K. (2008). Conceptual_fuel_channel_designs_fro_CANDU_-_SCWR.pdf.

Debrah, S.K., Ambrosini, W., and Chen, Y. (2013a). Discussion on the stability of natural circulation loops with supercritical pressure fluids. Ann. Nucl. Energy *54*, 47–57.

Debrah, S.K., Ambrosini, W., and Chen, Y. (2013b). Assessment of a new model for the linear and nonlinear stability analysis of natural circulation loops with supercritical fluids. Ann. Nucl. Energy *58*, 272–285.

DOENE (USDOE Office of Nuclear Energy, Science and Technology (NE)) (2002). A Technology Roadmap for Generation IV Nuclear Energy Systems.

Dutta, G., Zhang, C., and Jiang, J. (2015). Analysis of parallel channel instabilities in the CANDU supercritical water reactor. Ann. Nucl. Energy *83*, 264–273.

Ebrahimnia, E., Chatoorgoon, V., and Ormiston, S.J. (2016). Numerical stability analyses of upward flow of supercritical water in a vertical pipe. Int. J. Heat Mass Transf. *97*, 828–841.

Fukuda, K., and Kobori, T. (1979). Classification of Two-Phase Flow Instability by Density Wave Oscillation Model. J. Nucl. Sci. Technol. *16*, 95–108.

Ghadge, D.S. (2018). Analytical and numerical study of instability of supercritical water flowing upward in two heated parallel channels with wall thermal energy storage effects. Msc. Thesis, University of Manitoba. 131.

Hanna, B.N. (1998). CATHENA: A thermalhydraulic code for CANDU analysis. Nucl. Eng. Des. *180*, 113–131.

Hanna, B.N. (2010). CATHENA Simulation of supercritical heat transfer in a tube.

Hou, D., Lin, M., Liu, P., and Yang, Y. (2011). Stability analysis of parallel-channel systems with forced flows under supercritical pressure. Ann. Nucl. Energy *38*, 2386–2396.

IAE (2018). Global_Energy_and_CO2_Status_Report_2017.pdf.

Kalsi, P.S. DATA ACQUISITION (DAQ) AND CONTROL SYSTEM FOR SUPERCRITICAL CO2 EXPERIMENTAL LOOP. 74.

Leung, L.K.H., and Nava-Dominguez, A. (2017). Thermal-Hydraulics Program in Support of Canadian SCWR Concept Development. J. Nucl. Eng. Radiat. Sci. *4*, 011002-011002–011008.

Li, S., Chatoorgoon, V., and Ormiston, S. (2016). Numerical Instability Study of Supercritical Water Flowing Upward in Two Heated Parallel Channels. In MSc. Thesis 2016, Univeristy of Manitoba, H. Jiang, ed. (Singapore: Springer Singapore), pp. 187–200.

Li, S., Chatoorgoon, V., and Ormiston, S.J. (2018). Numerical study of oscillatory flow instability in upward flow of supercritical water in two heated parallel channels. Int. J. Heat Mass Transf. *116*, 16–29.

Liu, P., Hou, D., Lin, M., Kuang, B., and Yang, Y. (2014). Stability analysis of parallel-channel systems under supercritical pressure with heat exchanging. Ann. Nucl. Energy *69*, 267–277.

Sharabi, M., Ambrosini, W., He, S., Jiang, P.-X., and Zhao, C.-R. (2009). Transient Three-Dimensional Stability Analysis of Supercritical Water Reactor Rod Bundle Subchannels by a Computatonal Fluid Dynamics Code. J. Eng. Gas Turbines Power *131*, 022903.

Sharabi, M.B., Ambrosini, W., and He, S. (2007). Prediction of unstable behaviour in a heated channel with water at supercritical pressure by CFD models. Ann. Nucl. Energy *35*, 767–782.

Sharma, M., Bodkha, K., Pilkhwal, D.S., and Vijayan, P.K. (2015). A Supercritical Pressure Parallel Channel Natural Circulation Loop. 17.

Shitsi, E., Debrah, S.K., Agbodemegbe, V.Y., and Ampomah-Amoako, E. (2017). Numerical investigation of flow instability in parallel channels with supercritical water. Ann. Nucl. Energy *110*, 196–207.

Singh, M.P., and Singh, S. (2019). Non-linear stability analysis of supercritical carbon dioxide flow in inclined heated channel. Prog. Nucl. Energy *117*, 103048.

Su, Y., Feng, J., Zhao, H., Tian, W., Su, G., and Qiu, S. (2013). Theoretical study on the flow instability of supercritical water in the parallel channels. Prog. Nucl. Energy *68*, 169–176.

World Nuclear association (2019). Nuclear Power Today | Nuclear Energy - World Nuclear Association.

Xi, X., Xiao, Z., Yan, X., Li, Y., and Huang, Y. (2014a). An experimental investigation of flow instability between two heated parallel channels with supercritical water. Nucl. Eng. Des. *278*, 171–181.

Xi, X., Xiao, Z., Yan, X., Xiong, T., and Huang, Y. (2014b). Numerical simulation of the flow instability between two heated parallel channels with supercritical water. Ann. Nucl. Energy *64*, 57–66.

Xi, X., Xiao, Z., Yan, X., Xiong, T., and Huang, Y. (2014c). Numerical simulation of the flow instability between two heated parallel channels with supercritical water. Ann. Nucl. Energy *64*, 57–66.

Xiong, T., Yan, X., Xiao, Z., Li, Y., Huang, Y., and Yu, J. (2012). Experimental study on flow instability in parallel channels with supercritical water. Ann. Nucl. Energy *48*, 60–67.

Xiong, T., Yan, X., Huang, S., Yu, J., and Huang, Y. (2013). Modeling and analysis of supercritical flow instability in parallel channels. Int. J. Heat Mass Transf. *57*, 549–557.

Yi, T.T. (2004). A Linear Stability Analysis of Supercritical Water Reactors. J. Nucl. Sci. Technol. *41*, 11.

Zhang, L. (2017). Flow Instability Study of a Natural Circulation Loop with Supercritical Fluids. 204.

Zhao, J., Saha, P., and Kazimi, M.S. (2005). Hot-Channel Stability of Supercritical Water-Cooled Reactors—I: Steady-State and Sliding Pressure Startup. Nucl. Technol. *158*, 158–173.

(2014). Technology Roadmap Update for Generation IV Nuclear Energy Systems. 66.

(2017). World population projected to reach 9.8 billion in 2050, and 11.2 billion in 2100.